

THESIS

QUALIFICATION OF SILICON PHOTOMULTIPLIERS AND READOUT BOARDS
FOR USE IN PROTODUNE PHOTON DETECTORS

Submitted by

Connor Johnson

Department of Physics

In partial fulfillment of the requirements

For the Degree of Master of Science

Colorado State University

Fort Collins, Colorado

Spring 2018

Master's Committee:

Advisor: Norm Buchanan

Robert Wilson
Alexander Brandl

Copyright by Connor Johnson 2018

All Rights Reserved

ABSTRACT

QUALIFICATION OF SILICON PHOTOMULTIPLIERS AND READOUT BOARDS FOR USE IN PROTODUNE PHOTON DETECTORS

The study of neutrinos is a major component of modern High Energy Physics research. Neutrinos have been shown to have properties not predicted by the Standard Model, such as having non-zero mass. The Deep Underground Neutrino Experiment (DUNE) is a project in development which seeks to better understand neutrino physics. Part of the project includes designing a prototype detector for testing at CERN, which has been dubbed protoDUNE. Both DUNE and protoDUNE will consist of liquid argon time projection chambers, and a photon detection system. The photosensors used in the photon detection system will need to be submerged in cryogenic liquid, and will have to undergo thermal cycling as many as 5 times through their lifetime. The design installed in protoDUNE will use SensL C-Series SiPMs as photosensors, which have not been rated to operate below -40°C . This project sought to determine how these devices operate under repeated thermal cycles. Mounting boards were designed to measure the SiPM operation, and a cold test system was built which allows for repeated thermal cycling of these boards and their SiPMs. The data were closely examined to search for any issues arising, in particular searching for any problems consistent with damage to the SiPMs.

ACKNOWLEDGEMENTS

Thanks to my committee, my parents for always pushing me to succeed, and Kaitlyn for keeping me on the right track.

TABLE OF CONTENTS

Abstract	ii
Acknowledgements	iii
List of Tables	vi
List of Figures	vii
Chapter 1. Introduction	1
1.1. The Standard Model	1
1.2. Neutrinos	4
1.3. The Deep Underground Neutrino Experiment	5
Chapter 2. Photon Detection	11
2.1. Neutrino Detection	11
2.2. Liquid Argon Properties	12
2.3. Far Detector Neutrino Detection	14
2.4. Photon Detection	16
Chapter 3. Thermal Cycle Testing Apparatus	22
3.1. SiPM Devices and Test Boards	22
3.2. Cold Test System	24
3.3. SiPM Readout and the SiPM Signal Processor	27
Chapter 4. Experimental Results	33
4.1. SiPM Characteristics	33
4.2. Test Procedures	36

4.3. Testing Strategy	39
4.4. Test Analysis	42
4.5. Results	45
4.6. Testing Improvements and Issues.....	50
Chapter 5. Conclusions	53
Bibliography	56
Appendix A. Tested Boards.....	59
Appendix B. Excluded Data	70
Appendix C. Plots of Results from Thermal Cycling	72

LIST OF TABLES

3.1	Parameters for the SensL C-series devices as provided by SensL (at room temperature), and at cryogenic temperatures (77 K).....	23
3.2	SSP settings used in our testing. Full descriptions of these parameters are given in the SSP manual[1].	32
A.1	Devices tested for prototDUNE PD thermal qualification.....	63
A.2	Testing log for cycle boards.	66
A.3	Testing log for hoverboards.....	69
B.1	Excluded channels (cycle boards) not used in analysis along with rationale for exclusion.....	71

LIST OF FIGURES

1.1	Standard Model of Particle Physics.....	3
1.2	The two possible neutrino hierarchies (not to scale). $\Delta m_{21}^2 \approx 8 \times 10^{-5} \text{eV}^2$, and $\Delta m_{32}^2 \approx 2 \times 10^{-3} \text{eV}^2$	6
2.1	Liquid argon scintillation light produced by electron recombination[2].....	13
2.2	The TPC layout of a DUNE FD single phase module, showing the 3 APAs interleaved with 2 CPAs.....	15
2.3	The three wire planes making up a single APA. Not shown is an additional wire plane parallel with the collection plane, which is used for shielding and to improve the signal.	16
2.4	Light guide designs under consideration for the photon detection system.....	18
3.1	SiPM readout board designs.....	24
3.2	The internals of the test system before SiPMs are lowered. This shows the Cat6A cables connected to the board, which lead to the front panel as shown in Figure 3.4.	25
3.3	Thermal cycle test apparatus showing dark box (black box), test dewar (below the dark box), nitrogen supply (large steel container), and most connectors attached..	26
3.4	Front panel of the dark box, showing the external Cat6A cables which connect to the SSP. Each row corresponds to one CB, and only one may be read out at a time.	26
3.5	Internal mechanisms of the test apparatus. The white Cat6A cables connect to the CBs. The metal pipe is for filling the dewar with LN2. The black cable connects	

	to the depth sensor. Not visible in the cluster of Cat6A cables is a green LED and cabling for it.	28
3.6	Bulkhead for connecting to SiPMs. Each row corresponds to a “Block” on the mount. For CBs, the columns correspond to channels 0-3, 4-7, and 8-11 of the SiPMs on a CB, going from left to right.	29
3.7	Single waveform output for a single PE event. The SSP has a 150 MHz clock, so 1 unit on the x-axis corresponds to $6.67 \mu\text{s}$. The y-axis is in ADC units, which has a conversion of $6.60 \times 10^{-3} \text{ mV} / \text{ADC}$	30
3.8	This shows the two SiPM connection schemes. The newer SSP can take direct RJ45 connections, while the older version took quadrapus cables, which split the RJ45 connectors into the 4 individual channels.	30
4.1	Plot of pulse amplitudes, showing 1PE events (red) and events from greater than 1PE (blue).	36
4.2	Histograms for the pulse amplitude and integrated charge. Clear peaks are visible corresponding to 1PE, 2PE, etc.	37
4.3	Example closeup photograph taken of an SiPM before thermally cycling.	38
4.4	Total number of triggered events from an SiPM as a function of the threshold. The observed drop in events is due to the threshold cutting into the 1PE peak, where the beginning and end of the drop correspond respectively to the leading and trailing edge of the 1PE peak. The x-axis of this plot is in ADC, which can be directly converted to voltage by the conversion: $1\text{ADC} = 6.60\mu\text{V}$	41

4.5	Flow chart of procedures used for boards.	43
4.6	A pulse amplitude histogram, with peak locations and fits shown in red.	44
4.7	An integrated charge histogram, with two peak locations and fits shown in red. ...	44
4.8	Thermal cycle analysis for cycle board SN002-00003. The gain, dark rate, and crosstalk have been plotted for each of the 12 SiPM channels.	45
4.9	Example of high noise due to electronic “ringing” in the test system. Note that raising the threshold to remove the ringing would also remove events in the 1PE peak.	47
4.10	Example of high noise (the first peak) oversaturating the data, such that the PE peaks cannot be easily identified. In this case, the 1PE peak is fit, but no higher PE peaks are able to be identified in the data.	47
4.11	Flow chart of analysis procedure.	48
4.12	Close up image showing a SensL C-revision SiPM suffering thermal damage after being immersed in LN2.	51
C.1	03-600365C-SN00200002	72
C.2	03-600365C-SN00200003	73
C.3	03-600365C-SN00200004	73
C.4	03-600365C-SN00200005	74
C.5	03-600365C-SN00200008	74
C.6	03-600365C-SN00200010	75
C.7	03-600365C-SN00300003	75
C.8	03-600365C-SN00300004	76

C.9 03-600365C-SN00300007	76
C.10 03-600365C-SN00300008	77
C.11 03-600365C-SN00300009	77
C.12 03-600365C-SN00300010	78

CHAPTER 1

INTRODUCTION

This thesis begins with a discussion on the fundamental physics relevant for DUNE, and continues with an overview of DUNE and protoDUNE. Photon detection for protoDUNE is discussed, including liquid argon photon production. The thermal cycle testing system used for this research is explained, including the readout system. Parameters used to quantify operation are defined, followed by the results of the study. Finally, the implications of the study are discussed, as well as how the results are relevant to protoDUNE. My work for this study was focused largely on the data taking and analysis. I was responsible for programming the communication with our readout module, as well as analyzing the output to determine device parameters. Additionally, I played a large role in our overall cycle analysis. This included examining the results of our study to look for signs of thermal damage on the SiPMs, as well as work to determine when data could be safely excluded from our study.

1.1. THE STANDARD MODEL

The Standard Model (SM) of particle physics is an extremely accurate model of the fundamental particles and the forces between them - excluding gravity. Despite the success of the SM, it has been shown to be incorrect; or to be more precise, incomplete. The Deep Underground Neutrino Experiment (DUNE) will provide tools to study some parts of the SM better than any other similar experiment to date. This will lead to a better understanding of particle physics as a whole. As part of the plan leading up to DUNE, a prototype detector (protoDUNE) will be built and tested at CERN. The results of this will help to finalize the

design and components for the full DUNE experiment, and will serve to prove the viability of the full scale DUNE experiment.

Researchers in the field of High Energy Physics (HEP) have refined and studied the SM thoroughly, testing and refining the theory through many rigorous experiments. The SM was developed to explain the framework of the fundamental interactions of electromagnetism (EM), the strong interaction, and the weak interaction. One of the SM's biggest strengths is its ability to predict the interactions between the fundamental particles. A visual representation of the SM is shown in Figure 1.1 [3]. The quarks and antiquarks are the fundamental particles which combine to create all of the hadrons. These quarks are categorized by three pairs of particles, referred to as three generations. The pairs of quarks are as follows: up and down, charm and strange, top and bottom. These quarks in each pair have fractional charge of $+2/3 e$ and $-1/3 e$, respectively, where e is the magnitude of the electron charge. Likewise, the leptons consist of three pairs of particles, again referred to as generations. Each consists of a charged particle and a neutral particle with very low mass, the neutrino. We call the charged particles the electron, muon, and tau particle, and the neutrinos the electron neutrino (ν_e), muon neutrino (ν_μ), and tau neutrino (ν_τ), respectively. The quarks and leptons are all fermions, and together represent the twelve fundamental matter particles. In addition to these matter particles, there are four bosons which mediate the interactions between the particles, and an additional boson - the Higgs boson - which is responsible for the masses of the fundamental particles. The four interaction-mediating bosons consist of the photon, which mediates the electromagnetic (EM) interaction, the W^\pm and Z bosons, which mediate the weak interaction, and the gluons which mediate the strong interaction. The force of gravity is not described by the SM and has no corresponding boson, and attempts to explain

gravity with such a theoretical particle have not been successful. While the SM was able to predict many aspects of particle physics to extremely high accuracy, there are some aspects of it that are incorrect.

Standard Model of Elementary Particles

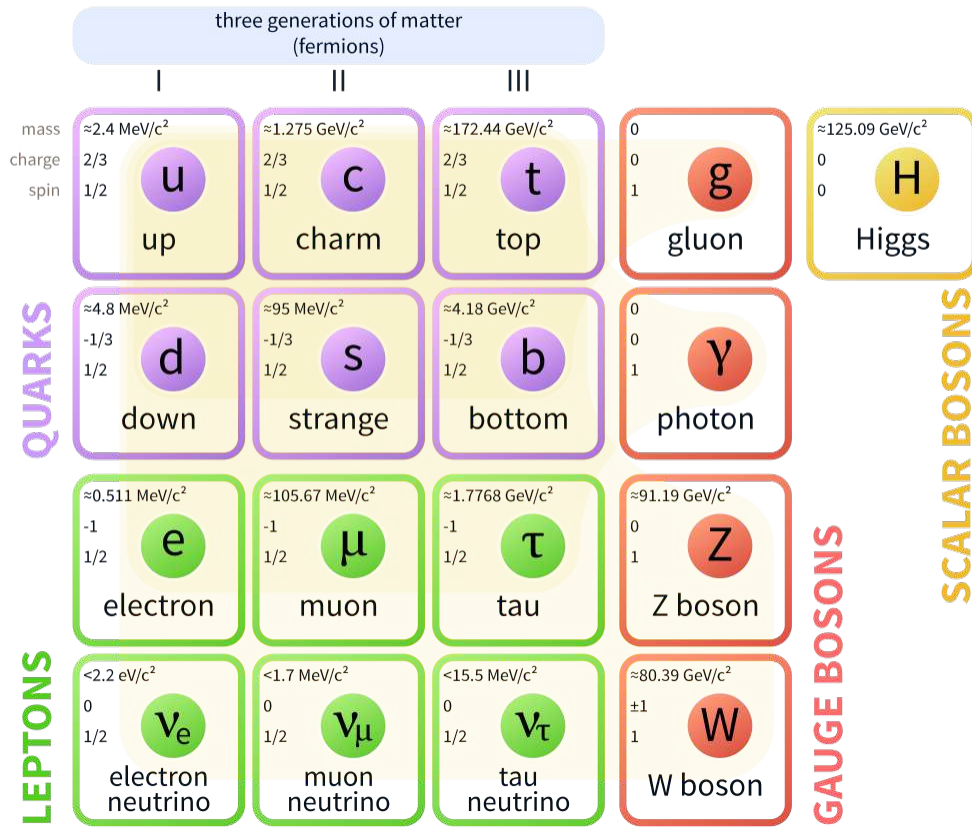


FIGURE 1.1. Standard Model of Particle Physics.

While the SM does an excellent job predicting fundamental and composite particles, it does not explain the masses or organization of particles. For instance, the model does not provide a good explanation for why particles come in three “generations”, or their mass hierarchy. This is a vital part of the SM, and has been utilized to make predictions in particle physics, but there is no strongly supported theoretical model for why precisely three generations exist. Additionally, the SM does not justify why particles have the masses we

observe. It provides a mechanism which leads to particle mass via the Higgs boson, but it does not explain why particles have their particular masses. One glaring flaw of the SM comes from specifics of how neutrinos behave. The SM requires that neutrinos be massless, but it has been shown that neutrinos do in fact have mass. This has been shown with the discovery of neutrino oscillations[4]. In order for neutrinos to oscillate, there must exist separate mass states, which exist as a superposition of neutrino flavor states.

1.2. NEUTRINOS

Neutrinos were first theorized by Pauli in 1930 as an explanation for strange behavior in β -decay experiments. During some very precise β -decay experiments, it was predicted that when measuring the final energy of the electron produced only a single energy would be detected due to energy conservation. In a normal two-body decay, the kinematics involved require specific energies of the released particles. In β -decay, this would mean the electron would have to be released with one specific energy. What was found instead was a broad spectrum of output energies. Pauli theorized that in order for the energy, momentum, and spin to be conserved, an additional hard-to-detect neutral particle was also emitted in the decay, taking some of the energy with it[5]. Many theories came about to explain this phenomenon, but Pauli's theory gained a lot of traction in the scientific community. This particle was eventually dubbed the neutrino (little neutral particle), and would be undetectable through electromagnetic interactions.

Many experiments helped to further a theory of neutrinos, such as the first direct detection of the anti-electron neutrino in the Cowan-Reines experiment[6]. This experiment detected antineutrinos produced from a nuclear reactor by searching for the interaction $\bar{\nu}_e + p \rightarrow e^+ + n$. The positron produced would quickly annihilate with an electron, and

produce two high energy photons to give a distinct signal showing antineutrino capture. As further experiments on neutrinos were carried out, however, many experiments found deficits in the expected number of neutrinos. One famous example is the Homestake experiment, which measured the number of neutrinos coming from the sun[7]. This experiment used J. Bahcall’s calculations for the predicted number of neutrinos earth should receive from the sun. Then using a large tank of perchloroethylene (a dry-cleaning fluid) measured the number of neutrinos interacting in the tank. When the experiment was performed, it observed around $1/3$ as many neutrinos as predicted. This was eventually understood to be a result of neutrinos oscillating between three distinct flavors.

1.3. THE DEEP UNDERGROUND NEUTRINO EXPERIMENT

Despite decades of experiments to better understand neutrinos, many questions remain. DUNE is designed to help answer some of these deeper questions. The answers will better describe neutrinos and their interactions beyond the SM, and lead to a better understanding of particle physics as a whole.

1.3.1. GOALS. While much is known about neutrinos, there are few known values for the mass states. The maximum values of the masses have limits, and the squared mass difference is known. However, the values of the masses are not known to much precision, and the mass ordering (or “hierarchy”) is not known. Determining the ordering will help to support or exclude theories beyond the SM, which rely on a particular neutrino mass hierarchy. In addition to the values for the masses, the fraction of flavors that make up the mass states is not known to high precision. Another important goal of DUNE is to determine the amount of Charge-Parity (CP) violation in neutrinos, which will help to describe the matter-antimatter

asymmetry in the universe. These measurements will provide more precise values of neutrino oscillation, as well as measurements based off these oscillations.

Massive neutrinos are not allowed by the SM, and therefore are an obvious choice to research physics beyond the standard model. The masses have been heavily limited in magnitude (to be much lighter than any other type of massive particle), but as of yet there is no known way to measure the exact mass values. The most useful part of neutrino masses we know how to measure as of now is the mass ordering of the particles. This is defined as the mass hierarchy of the neutrino mass states: ν_1 , ν_2 , and ν_3 . Experiments finding the differences in masses Δm_{21}^2 and Δm_{32}^2 have concluded only two possible orderings of neutrinos. We define them as the “normal” ($\nu_1 < \nu_2 < \nu_3$) and “inverted” ($\nu_3 < \nu_1 < \nu_2$) mass hierarchies, shown in Figure 1.2. Many theories beyond the SM predict a normal hierarchy, while some predict an inverted hierarchy. This determination would help to exclude theories which predict the wrong hierarchy.

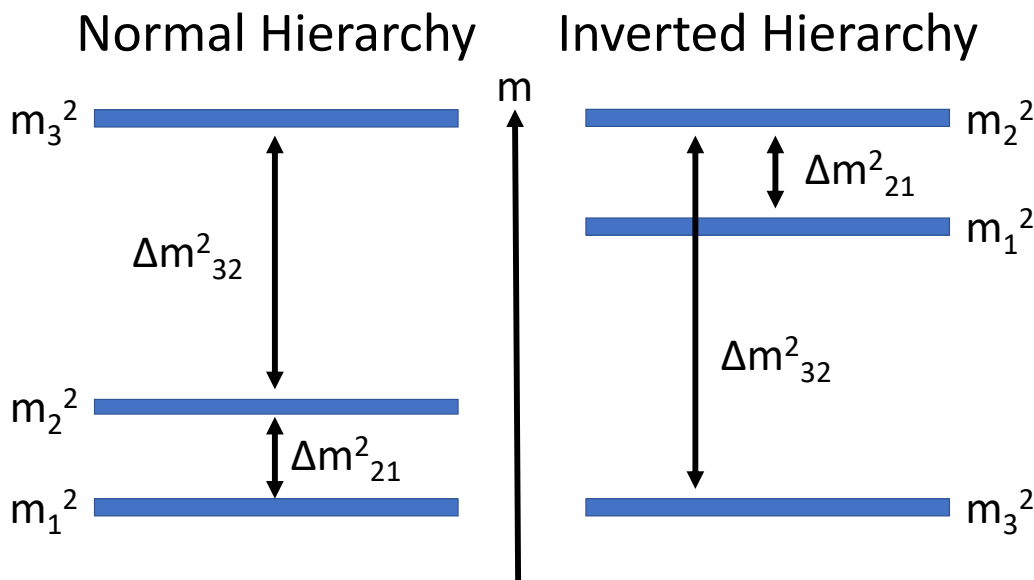


FIGURE 1.2. The two possible neutrino hierarchies (not to scale). $\Delta m_{21}^2 \approx 8 \times 10^{-5} \text{eV}^2$, and $\Delta m_{32}^2 \approx 2 \times 10^{-3} \text{eV}^2$.

The concept of CP violation is well understood, but its origin in the SM and the exact amount of violation is not. Charge conjugation describes flipping the charges of all particles in a system, while parity conjugation describes inverting the spatial coordinates of the system. The combination of these two steps describes CP conjugation. Parity alone was found to be violated in Cobalt-60 decay in the year 1957[8]. After this discovery, CP conjugation was suggested as a possible conservation law. This was well received, but since then several examples of CP violation have been found in nature. Among the first experimental evidence of CP violation was the Fitch-Cronin experiment[9]. This result showed that CP violation occurs in the decay of neutral kaons.¹ The CP violation in kaons is in fact allowed by the SM, and it is believed that this CP violation will likewise appear with neutrinos. The amount of violation is described by a parameter referred to as δ_{CP} . Oscillation experiments such as DUNE will be sensitive to this measurement, and will help to better determine its value. The value is unknown as of now, but there is evidence that the CP violation is “maximized”, i.e. the phase is purely imaginary. This is one of the many things that may be determined by data taken at DUNE.

1.3.2. NON-BEAM PHYSICS. The neutrino beam for DUNE will be produced at Fermilab, and will be sent through the near and far detectors. This beam of neutrinos will be studied to make measurements to help determine the main physics goals of DUNE. In addition to these neutrino characteristics, a goal of DUNE will be to analyze non-beam physics. This refers to events of interest in the detector due to something other than neutrinos from the beam. Two examples of this include searching for supernova neutrinos, as well as looking for evidence of proton decay. These studies are the main reason a photon detection system

¹Charge-Parity-Time (CPT) conjugation is now believed to represent a conservation law, but testing this is significantly more challenging due to having to test processes under time-reversal.

is important for DUNE, while protoDUNE will help to test and compare photon detector designs. This is described in greater detail in Section 2.4.

When a star undergoes a core-collapse, 99% of the energy released is in the form of neutrinos and anti-neutrinos[10]. The number of neutrinos released is so large that even given the vast distances involved and the low interaction rate, they will still interact with our neutrino detectors in an observable amount. At the start of the core collapse itself, the neutrino burst occurs in a matter of seconds. However, the high temperature, density, and pressures involved serve to slow the release of photons due to a high interaction rate. This leads to the neutrino burst from a supernova arriving before the visible light from a supernova, typically on the order of hours[10]. Not only will analysis of the neutrino events help to better understand the inner workings of a supernova, it also provides an early warning trigger to where a supernova is about to be visible. Many active neutrino detectors including Super-K, Ice Cube, KamLAND, and Daya Bay are part of a joint operation called the SuperNova Early Warning System (SNEWS) which seeks to use such neutrino bursts to detect supernovae before they are visible. In addition to this burst, stars provide another signal when close to collapse in the form of fusing silicon. Once silicon begins to fuse into iron, a star typically has only a matter of days before undergoing collapse. It is estimated that this process would also produce neutrinos at a high rate, and provides an alternative way to predict supernovae. This would allow warning on the order of days, allowing even more time to get as many telescopes as possible pointed at possible locations for supernovae.

In addition to supernova searches, the non-beam goals for DUNE include the study of proton decay. Placing the detector deep underground greatly reduces the amount of cosmic rays in the detector. This allows for a greater sensitivity to search for more rare events such

as proton decay[11]. Proton decay has not been detected as of yet, but is part of many theories beyond the standard model. Such a discovery would prove that Baryon number conservation can be violated, which would lead to a better understanding of the formation of the universe. Many grand unified theories (GUTs) and supersymmetry theories predict some form of proton decay, typically with a theoretical lifetime of over 10^{31} years. One common predicted decay mode is $p \rightarrow e^+ + \pi^0$ [12]. The DUNE experiment has the possibility to detect this, but not at a rate better than other experiments. However, the DUNE experiment will be highly sensitive to possible proton decay modes which result in a final state K^+ particle, such as the decay mode $p \rightarrow K^+ + \bar{\nu}$. This decay would produce a K^+ with an energy in the range of 100 MeV, which DUNE can detect at high efficiency[11, 12]. While such goals are secondary to some of the main neutrino measurements, both supernova studies and proton decay have the potential to be groundbreaking physics research which cannot be ignored.

1.3.3. DUNE DESIGN AND PROTODUNE. The experiment will consist of two facilities; a so called “Near” detector located at Fermilab, and a “Far” detector to be built at the Sanford Underground Research Facility in Lead, South Dakota. A focused and high-energy beam of neutrinos will be created using the main injector at Fermilab, and sent through the near detector. It will then travel 1300 km through the ground towards the far detector. Measuring the number of ν types at each detector will provide the ability to determine oscillation parameters.

As part of the development for DUNE, it is important to keep clear goals and milestones to ensure the project will succeed. One such milestone is a working prototype of the detector systems. This prototype, dubbed protoDUNE, is currently being constructed in the EHN1 facility at CERN. The protoDUNE will consist of full-scale detection systems similar to the

ones which will be used for DUNE. This will allow for a test of all parts of the detection systems, and ensure that they all work well together.

Two overarching designs exist for the far detector. A single-phase Time Projection Chamber (TPC), and a dual-phase TPC. The single-phase design will be focused on using only liquid argon for detection. The dual-phase design, however, will utilize a layer of gaseous argon in addition to the liquid argon, and examine electrons accelerated through the gas. One of the main things the two protoDUNEs will allow us to do is test out both of these designs, and determine how well they work compared to each other. Our study, however, is focused solely on the single-phase design, and any references to the detection system refer to the single-phase TPC design.

The current plan for protoDUNE is very aggressive. Construction is underway, and the experiment aims to be up and running by the fall of 2018. The results of protoDUNE will help to determine the final designs for DUNE, so it is important that protoDUNE is built and running quickly. While protoDUNE isn't intended to answer many deeper physics questions, it is critical in determining the final design for DUNE. Every component of the full system must have been thoroughly tested and confirmed, so protoDUNE can show all the pieces work together. The results from the protoDUNEs will help to determine the best designs moving forward with DUNE, and will help to describe the capabilities of the detector systems.

CHAPTER 2

PHOTON DETECTION

Due to the low rate of interaction, neutrino detection faces unique challenges. There is no way to directly detect neutrinos, since they do not interact via the electromagnetic interaction. Instead, experiments examine particles resulting from weak interactions to determine the physics of the primary interactions. The core components of DUNE are the two particle detector systems. The far detector will be composed of two separate subsystems; a Time Projection Chamber (TPC) which detects electrons from ionization, and photon detectors. Our work at Colorado State University has been focused on the design and prototype testing for the photon detection system. We have studied Silicon Photomultipliers (SiPMs), specifically how cryogenic cycling will effect their operation and characteristics.

2.1. NEUTRINO DETECTION

Neutrino detection is not trivial. Since neutrinos interact only via the weak force, they can pass through a large amount of matter before interacting at all. While many types of neutrino detectors exist, all rely on having a target with a large amount of mass, and a large enough neutrino flux so that events occur as often as possible. Even with the largest detectors and an intense beam of high energy neutrinos, events will still occur relatively rarely. The Cowan-Reines experiment in the 1950's, for example, found that with a flux of 5×10^{13} antineutrinos per square centimeter per second, less than 3 interactions would be expected in a full hour of testing[6, 13]. Due to this low interaction rate, it is critical that any neutrino detector is able to record neutrino events with high efficiency. Two examples used in current experiments are Water Cherenkov and Scintillators[14, 15].

Water Cherenkov detectors consist of a large tank of water, surrounded by many Photomultiplier Tubes (PMTs). They utilize and observe Cherenkov light, which is a phenomenon that occurs when charged particles travel faster than the local speed of light in a medium. Since these detect very fast moving particles, the threshold energy of particle detection is relatively high compared to other detector designs. Another common form of detectors are scintillators, which were one of the first methods utilized to detect neutrinos. Most generally, scintillators are some transparent medium which releases light when excited by a particle that travels through and interacts. The Cowan-Reines experiment is one example of using scintillators to observe neutrinos[6]. More recently, neutrino detector designs have moved towards Time Projections Chambers (TPCs), and in particular liquid argon TPCs. The general TPC design was first proposed in 1977 by Carlo Rubbia, and has been used in such experiments as ICARUS, which began operation in 2010, and MicroBoone, which began operation in 2015[16].

2.2. LIQUID ARGON PROPERTIES

Liquid argon is an excellent ν -detection medium for several reasons. When energetic particles travel through liquid argon, photons are released. Electrons are excited out of their ground state by particles traveling through, and one of two things will happen. If the energy they receive is higher than their binding energy, the free electrons will drift to an anode to be detected. If they do not have enough energy to be released, or if a free electron is captured by an ionized Ar_2^+ molecule, they will undergo recombination. A diagram of this process is shown in Figure 2.1. This process lets the electron fall to a lower energy state, while releasing a photon in in the vacuum ultraviolet (VUV) range. Due to the energy levels in argon, this light will have a wavelength of 128 nm at a rate of approximately 40,000 photons per MeV

of deposited energy[11, 17]. Argon is almost completely transparent to this 128 nm light, so the light can travel freely to light guides distributed through the detector.

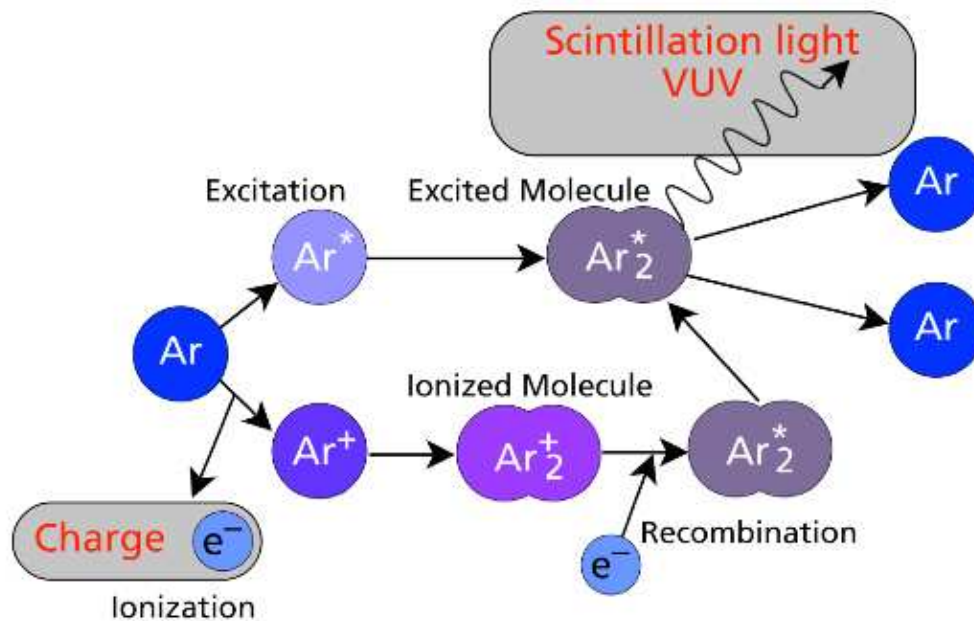


FIGURE 2.1. Liquid argon scintillation light produced by electron recombination[2].

Another advantageous property of argon is how well electrons flow through it. Argon is a noble element, meaning that electrons can flow mostly unimpeded through it even in a liquid phase. This can be used to “drift” free electrons through the detector simply by applying an electric potential. Impurities in the liquid argon can interfere with this drifting process and allow the electrons to recombine prematurely, so the LAr used in TPCs must have impurities below one part per billion[11]. The detector is split into cells, consisting of two sets of wire planes to detect the charged particles. The two wire planes are referred to as the cathode plane assembly (CPA) and anode plane assembly (APA), and are used to give spatial position (x,y) of the charged particles in the TPC. The z-component of the charged particle position is determined by the the timing and drift velocity of the particles.

Two other important benefits of liquid argon are its cheapness and availability. Liquid argon can be bought in bulk for relatively low cost in large amounts. Since DUNE will use four 10 kt modules filled with liquid argon, the material cost for the fiducial volume is not trivial. Using liquid argon will help to keep the cost of the ν -detection medium reasonable. Additionally, liquid argon is readily available in large quantities, and it won't be especially difficult to obtain the necessary amount. DUNE will utilize the properties of liquid argon to obtain high precision measurements of particle trajectories. Drifting electrons will allow for high precision location of events, while light guides will capture scintillation light to help with event timing, in particular with non-beam events. The following section will discuss the specifics of how DUNE will utilize these properties of liquid argon to serve as a good neutrino detector.

2.3. FAR DETECTOR NEUTRINO DETECTION

DUNE's far detector (FD) will allow examination of the neutrino oscillation. While the near detector (ND) will examine the beam as it is produced, the FD at Sanford will determine how the characteristics of the neutrino beam evolve in time, and in particular how the neutrino flavor changes. As stated above, the two components of the far detector are a TPC, and a photon detection system.

2.3.1. TIME PROJECTION CHAMBER. The layout of DUNE's far detector will be a system of TPC cells. The active volume of a 10 kt module will be 12 m vertically, 14.5 m horizontally, and 58 m long in the direction of the beam. The cross-section along the beam axis can be seen in Figure 2.2. APAs are on either side of the fiducial volume, as well as in the center, for a total of three across, defining two TPC cells. Two CPAs are interleaved between the APAs. The APAs are 6 m high, so two such modules will be stacked vertically

to fill the 12 m active volume. A relative voltage of +180 kV will be applied to the APA, corresponding to a voltage differential of 500 V/cm. While neutrinos are chargeless, the particles resulting from interactions are often charged. Among the common interactions are $\nu_\mu + n \rightarrow \mu + p$ and the inverse $\bar{\nu}_\mu + p \rightarrow \bar{\mu} + n$.¹ The released μ will liberate atomic electrons as it travels through the liquid argon. Due to its high mass compared to the electron, it will travel relatively straight with a long track. The μ will slow down as it travels until either undergoing muon decay ($\mu \rightarrow \nu_\mu + e + \bar{\nu}_e$), or escaping the detector.

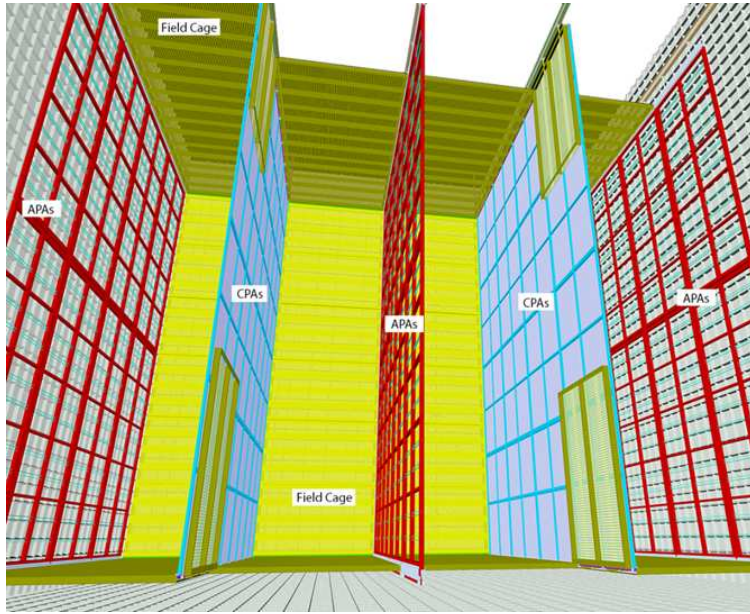


FIGURE 2.2. The TPC layout of a DUNE FD single phase module, showing the 3 APAs interleaved with 2 CPAs.

The released electrons drift to the APA at a timescale of around 3 ms[11]. A series of parallel wire anodes will lie in a plane, and detect electrons passing through by induction while letting them continue. These wires have approximately 5 mm separation, and the separation between planes is also approximately 5 mm. This is shown in Figure 2.3. After the electrons pass two such planes (referred to as the U and V planes), a final series of

¹The neutrino beam is produced as ν_μ or $\bar{\nu}_\mu$. There will be ν_e and ν_τ in the beam due to contamination and oscillation, but the beam will be primarily ν_μ .

parallel wire anodes will collect the electrons. The first two wire planes are referred to as the induction planes and lie at an angle of $\pm 35.7^\circ$ from vertical, and the third is referred to as the collection plane and lies vertically. Additionally, there is a 4th wire plane not shown, with wires parallel to those in the collection plane, and lies before the other three planes. This additional plane serves as shielding, and improves the signal picked up by the other wire planes. This wire plane system provides DUNE with high accuracy tracking of charged particles traveling through the liquid argon.

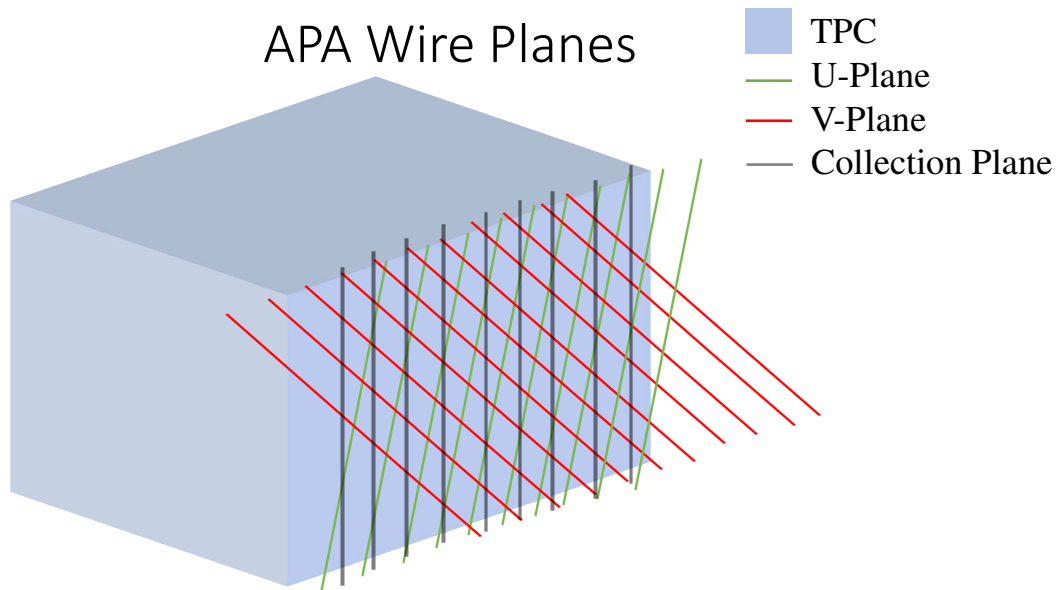


FIGURE 2.3. The three wire planes making up a single APA. Not shown is an additional wire plane parallel with the collection plane, which is used for shielding and to improve the signal.

2.4. PHOTON DETECTION

The photon detection system is separate from the TPC, and serves to improve calculations for non-beam events. These non-beam events include searching for supernova neutrinos as well as proton decay, as described in Section 1.3.2. For events resulting from beam, the

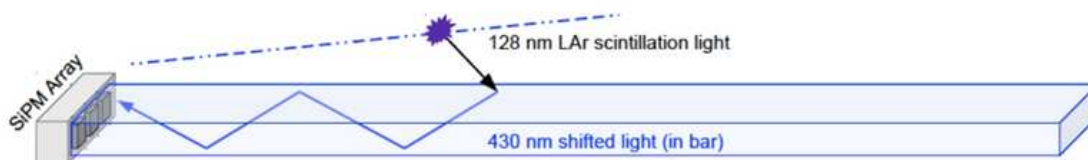
timing is known to the precision of a few μs . This is due to the beam “spill” (one pulse of neutrinos) being limited to a few μs . For non-beam events, however, the time of events (t_0) is not known. The main disadvantage of this is that this leads to very low resolution on the energy deposition $\frac{dE}{dx}$. The $\frac{dE}{dx}$ is critical for many analyses, including particle identification. The photon detection system will allow precise timing for t_0 and in turn better resolution on $\frac{dE}{dx}$.

2.4.1. LIGHT GUIDES. The liquid argon is transparent to the 128nm light produced by the recombination process. The 500 V/cm electric field will slightly impact the expected rate of photon production, so instead of the previously mentioned 40,000 photons per MeV of deposited energy, the rate will be closer to $\sim 20,000$ photons per MeV[11]. The design for the photon detector is based around a light guide with wavelength shifters combined with photosensors. These light guides are long and thin rectangular bars placed inside the cryostat. When the photons hit the bar, they will be wavelength shifted and be captured by the light guide. Once inside the bar, the light travels through total internal reflection towards the end of the bar. Photosensors are placed at the end of these bars, which are read out directly by the data acquisition (DAQ) system.

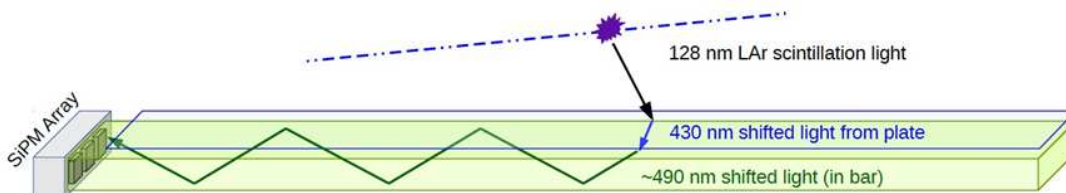
Two designs for the light guides are currently under consideration. The first was designed at the Fermi National Accelerator Laboratory (FNAL). This FNAL design uses bars made of acrylic, which are coated in a wavelength shifting material known as tetraphenyl butadiene (TPB), as shown in Figure 2.4a. As the 128 nm photons strike the bar, they are absorbed by the TPB and 430 nm photons are emitted. The efficiency of this is only around 50%. These 430 nm photons are then propagated towards the photosensors. An alternative light guide was designed by Indiana University (IU), shown in Figure 2.4b. This design uses radiator

plates which lie on the front and back faces of the light guide, which are coated in TPB. These radiator plates shift the photons to 430 nm, before the light strikes the bar itself. The bar itself is made of a material called Y11, which further shifts the photons to ~ 490 nm.

It is uncertain which of these two designs will provide higher efficiency. The photosensors to be used in protoDUNE are better tuned for the 490 nm light from the IU bars. However, there are additional efficiency losses during the second wavelength shift to 490 nm. It is uncertain whether the better tuning of the wavelength will make up for the extra losses from the second wavelength shift. Both designs will be tested in protoDUNE, which will help to determine which design is better for the photon detection system in DUNE.



(A) FNAL design TPB-coated light guide.



(B) IU design Y11 light guide with radiator plates.

FIGURE 2.4. Light guide designs under consideration for the photon detection system.

Note that there are other losses in this system which are taken into account. Since the light can travel one of two ways once inside the bars, and photosensors will only be located at one end, there is a 50% drop in efficiency due to the two directions the light can go. Potential design improvements of the photon detector system address this by reflecting or redirecting the photons back to the sensor end. The geometry of the photon detector module also lowers

the photon acceptance. Each cell of the TPC will have 10 photon detector modules attached to the CPAs, and a single photon detector module covers an area of $2.2 \text{ m} \times 83 \text{ mm}$. This results in a relatively low covering of photon detectors, and a large loss in photon detection.

2.4.2. PHOTSENSORS. Two main types of device used for photon detection are Photomultiplier Tubes (PMTs) and SiPMs. PMTs were the main device used for photon detection for many years. These have been improved over time, and currently give high accuracy detection of single photons with a quantum efficiency of $\sim 30\%$ [18]. PMTs function using an avalanche effect; a single incident photon of high enough energy will excite an electron via the photo-electric effect. If the electron has enough energy to overcome its binding energy, this free electron causes a cascade of electrons through several high voltage (HV) stages called dynodes. The result is large shower of electrons which can be easily detected.

PMTs have been used for many years, and have consistently proven useful. They come with some disadvantages, however, which led to a search for new detectors. One critical issue with PMTs is their bulkiness. Traditionally, the electron cascade occurred across a long tube, hence the name. While nowadays varying sizes of PMTs exist, most common PMTs on the market are relatively large. A somewhat extreme example are the PMTs used in the Super-K experiment. These detectors have a diameter of 20" [14]. While many PMTs are much smaller than this, PMTs do tend to be significantly larger than SiPMs. Despite their good detection capabilities, this size leads to several complications. It is difficult to place these large devices near where the events occur, leading to these devices often being placed on the edges of the detector. Additionally, it prevents multiple detectors from being placed near each other. Both of these lead to PMTs doing a very poor job at giving spatial information. These devices also are very expensive, and placing them throughout the length

of a long detector like DUNE would prove cost prohibitive. Also, PMTs generally function at around a voltage of 1 kV, which can prove difficult for both technical and safety reasons[19].

SiPM devices provide an alternative in photon detection. Similarly to PMTs, SiPMs are photomultiplier devices. Unlike PMTs, however, SiPMs utilize semiconductor properties to undergo avalanche. The SiPM acts as a diode in breakdown, using the principle of an avalanche photo-diode (APD). When a photon is absorbed by the device, it excites an electron and allows current to flow. The device then undergoes quenching to return to its nominal state. This alone leads to several benefits over traditional PMTs. The voltage requirements are generally less than for PMTs. SiPMs are solid state devices, and can function at much lower operating voltages. The breakdown voltages required will vary based on device type and temperature, but typical operating voltages are less than 30 V. Another advantage of these devices is that they are much more compact. These lower space requirements solve two problems with PMTs; it allows them to be placed in a way to better capture produced photons, and allows for enough photon detectors to determine position information with much higher accuracy. Finally, the SiPMs are simply much cheaper than equivalent PMTs. SiPM devices can be as cheap as \$30 per unit, as opposed to \$300-\$1000 per unit for PMTs.

Due to these advantages, protoDUNE will utilize SiPM devices as its photosensors in the photon detection system. There are some problems that need to be addressed before this is done, however. Most SiPMs are only intended for operation in a specific temperature range. For DUNE and protoDUNE, however, the devices will be required to operate from inside the cryostat which is filled with liquid argon. That means these detectors will have to function at the temperature of liquid argon, ~ 87 K. Few of these devices have been tested thoroughly under these conditions, so it is not certain whether they will still function as required. One

of the main issues is how thermal cycling would affect their operation. It is a possibility that transferring them from cryogenic temperatures to room temperature and back could cause thermal stresses and damage their operation or mechanical structure. This needs to be examined closely to determine if this could cause problems using them at protoDUNE.

CHAPTER 3

THERMAL CYCLE TESTING APPARATUS

This chapter describes the SiPMs and readout boards, as well as the apparatus used to qualify them for operation in protoDUNE. While many designs of SiPMs exist, the specific SensL devices have several benefits, including their size, relative cheapness, and operating characteristics. They have an efficiency of 41%, and have good after-pulsing behavior[11]. However, it was not known how well they would operate under cryogenic conditions such as those they will be exposed to inside protoDUNE.

3.1. SiPM DEVICES AND TEST BOARDS

The devices examined in this study are SensL C-Series 6mm \times 6mm surface mount SiPMs. The room temperature operating characteristics of these devices are described in a datasheet provided by SensL[20]. Table 3.1 shows a comparison of some SensL provided values for the device parameters at room temperature, and typical values while in cryogen[20]. These devices are the reference design photosensors for the protoDUNE photon detectors. The devices are mounted to a test readout board, though the board design differs for these tests and for protoDUNE. The devices and mounting boards at DUNE are expected to be thermally cycled in liquid argon (LAr) around four times in the course of their operation. This study was performed to determine the effects of this thermal cycling on both the SiPMs and their mounting boards.

The basic design of readout boards are custom designed 6-layer printed circuit boards (PCBs). These PCBs were designed at CSU, and manufactured by Advanced Circuits. The SiPMs were mounted on the boards at CSU, using the process outlined in the Quality Control

TABLE 3.1. Parameters for the SensL C-series devices as provided by SensL (at room temperature), and at cryogenic temperatures (77 K).

Parameter	Warm value (SensL datasheet)	Cold value
Breakdown Voltage (V)	24.2 - 24.7	20
Gain	3×10^6	4×10^6
Dark rate (Hz)	1.2×10^6	10
Crosstalk (%)	7 (at $V_{breakdown} = 2.5$ V)	20 (at $V_{breakdown} = 5.0$ V)

Procedures technical note[21]. The SiPMs were placed on the board with a precision of 100 μm . Two different board designs are used for SiPM readout. The “cycle boards” (CBs) are 3” \times 3” PCBs, with 4 rows of 3 SiPMs each, for a total of twelve SiPM devices per board, and are shown in Figure 3.1a. These boards were designed to be read out by three Cat6A cables with RJ45 connectors, one placed above each column of SiPM devices. The RJ45 connectors allow readout of each SiPM. This design is shown in Figure 3.1a, and this board design is the focus of this study. While this board design is different than what will be used in protoDUNE, it provides a way to examine each SiPM individually. The quality assurance (QA) process is greatly simplified by being able to examine individual devices. For this reason, the majority of testing was done using this board design.

The official readout design passively “gangs” groups of three SiPM devices, such that their output is sent to the same readout channel. Technical details can be found in the technical note[21]. Boards using this design are referred to as “hoverboards” (HBs), and the design is shown in Figure 3.1b. Twelve SiPMs are placed in a single row, with four groups of three SiPMs ganged together. This results in a HB having four readout channels, which are read out from a single RJ45 connector and Cat6A cable. Since the devices are ganged together, it is not possible to determine which individual SiPM is being read out at a given time. While this makes QA determination more difficult, this is the same design which will be used for photon detectors in protoDUNE. It was critical to determine if the SiPM

characteristics are consistent through thermal cycles, both when examined individually and when ganged together. This thesis is focused on the cycle board tests.

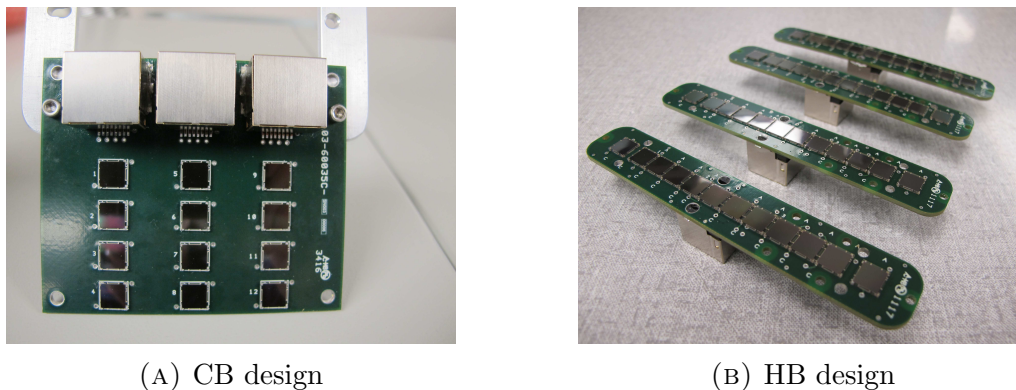


FIGURE 3.1. SiPM readout board designs.

3.2. COLD TEST SYSTEM

The test system, colloquially referred to as the “Little Dipper”, for the thermal cycle tests is based around a 40 L dewar. While DUNE and protoDUNE will have modules filled with LAr, this system uses liquid nitrogen (LN2) instead. As previously explained, LAr serves well as a target for neutrino detection. LN2 has a boiling temperature very close to that of LAr; 77 K and 87 K, respectively. By using LN2 instead of LAr, the thermal shock on the devices should be at least as great as it will be for protoDUNE. Therefore, if the SiPMs do not fail under the thermal shock of LN2, we can be fairly confident they should handle the shock for LAr. Additionally, since LN2 does not produce scintillation light, events resulting from cosmic rays won’t complicate the results. This makes it much simpler to study the SiPM devices themselves, namely the “dark counts”. Dark counts are the result of a spontaneous avalanche in one cell of the photosensor. The rate of this occurrence is temperature and bias voltage dependent, and in cryogenic liquid this rate is much lower than it would be at room

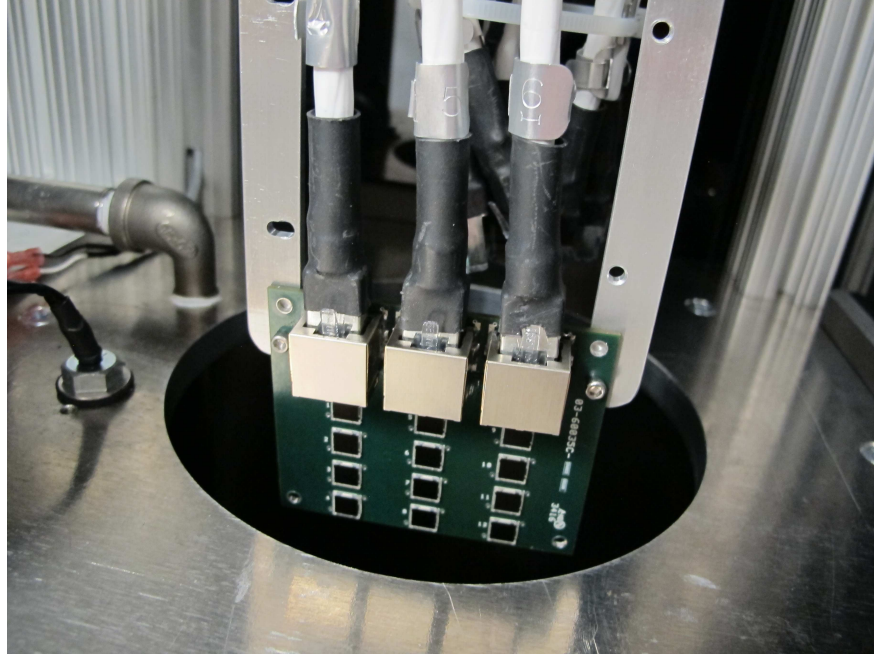


FIGURE 3.2. The internals of the test system before SiPMs are lowered. This shows the Cat6A cables connected to the board, which lead to the front panel as shown in Figure 3.4.

temperature, at approximately 10 Hz in LN2[11].¹ One other significant reason to use LN2 as opposed to LAr is simply due to price. LAr is relatively cheap for a target in neutrino experiments (a few dollars per liter), but costs can get high if it is not being recycled. LN2 is significantly cheaper (around \$0.10 / liter), which makes it an even better choice of cryogenic liquid for our tests.

The test system is housed around a large light-proof box, shown in Figure 3.3. Up to four boards at a time were attached to a holder designed to have CBs or HBs mounted. An example of this with a single CB mounted is shown in Figure 3.2. The boards were then very slowly lowered by a stepper motor into the dewar. As the mount reaches the top of the dewar, a seal is formed to prevent light leaking in. By not having scintillator and blocking background photons, we can examine only the dark counts produced inside the

¹The dark rate for these devices at room temperature is listed as 1.2 MHz by SensL[20].

SiPMs. In the event we do wish to look at controlled photon events for cross-checks, an LED is mounted inside the dewar. This setup allows for high control of most variables, and allows an examination of how thermal cycling the SiPMs will change their characteristics.



FIGURE 3.3. Thermal cycle test apparatus showing dark box (black box), test dewar (below the dark box), nitrogen supply (large steel container), and most connectors attached.

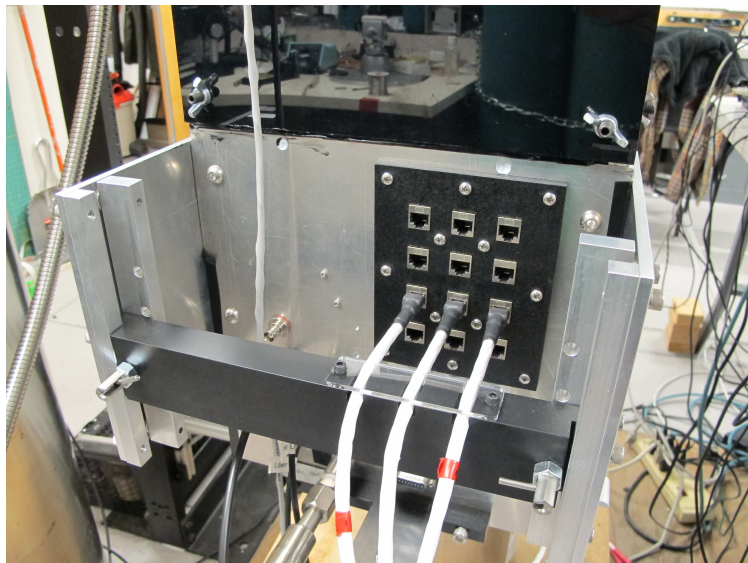


FIGURE 3.4. Front panel of the dark box, showing the external Cat6A cables which connect to the SSP. Each row corresponds to one CB, and only one may be read out at a time.

The top of the mount has added feedthroughs built in for cryogen plumbing, SiPM cabling, depth monitoring, as well as a cable for optionally pulsing an LED installed inside the dewar. Twelve Cat6A cables were installed through the inner mounting system to connect the readout boards to the front of the dark box. This internal structure can be seen in Figure 3.5. Outside the dewar and mounting module, these feedthroughs attach to a front panel of the little dipper. This panel is shown in Figure 3.4, including all of the various connectors. The tank of LN2 shown on the left has two lines to the little dipper; the metal pipe flows LN2 while the black hose flows gaseous nitrogen. By flooding the inside of the dewar with nitrogen gas, the air inside is pushed out. This prevents water vapor from condensing and freezing on any of the electronics or mechanisms inside. Two limit switches are used to stop the stepper motor when the mount is at the correct depth when raising or lowering the test boards. One more connector is used to measure the depth of liquid nitrogen inside the detector. The bulkhead, as shown closer in Figure 3.6, is where the cabling for the SiPMs connects.

3.3. SiPM READOUT AND THE SiPM SIGNAL PROCESSOR

SiPM readout is done by reading the analog signal from the SiPMs, selecting events which pass a trigger threshold, and digitizing this information for processing. The output from the device is relatively simple. After a bias is applied, the output voltage of the SiPM will remain relatively constant until a photon is detected. Once this happens, the voltage will jump, and then slowly return back to where it was. This voltage return time typically takes on the order of $\frac{1}{2} \mu s$. This is shown in Figure 3.7. A SiPM Signal Processor (SSP) is utilized to determine when an SiPM has triggered. It constantly samples each SiPM, and determines when an event has occurred based on a trigger threshold provided by the user.

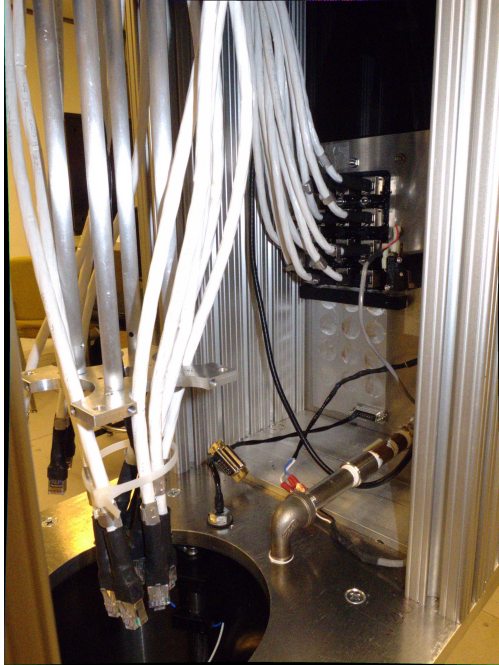


FIGURE 3.5. Internal mechanisms of the test apparatus. The white Cat6A cables connect to the CBs. The metal pipe is for filling the dewar with LN2. The black cable connects to the depth sensor. Not visible in the cluster of Cat6A cables is a green LED and cabling for it.

The SSP served as the readout system, sampling the raw analog output from the channels and outputting digital event information. For the CBs, one channel corresponds to a single SiPM. Partway through testing, the SSP was upgraded to a newer model. These two SSPs used different cabling to connect to the front panel of the dark box. The first SSP used twisted pair cables with LEMO connectors, referred to as “quadrapus” cables. This is shown in Figure 3.8a. These split the 4 channels in a Cat6A cable into 4 separate channels, with each SiPM corresponding to a single LEMO connector. Since each CB has three connectors, this setup mapped the twelve SiPMs to twelve separate LEMO inputs to the SSP. This SSP was replaced with the upgraded model on January 11, 2017, which was able to internally separate the four channels in a single Cat6A cable into four separate channels. The upgraded SSP took three RJ45 connectors as input, and used twisted pair Cat6A cables with RJ45



FIGURE 3.6. Bulkhead for connecting to SiPMs. Each row corresponds to a “Block” on the mount. For CBs, the columns correspond to channels 0-3, 4-7, and 8-11 of the SiPMs on a CB, going from left to right.

connectors on both ends to connect to the front panel of the dark box. The upgraded SSP is shown connected in Figure 3.8b, above the original SSP (unconnected).

The SSP serves as a separate processor for the raw data and determines when a SiPM has triggered, as well as values which describe the event. The SSP reads out the voltage from each channel once every clock cycle. The clock of the SSP operates at 150 MHz, so one clock cycle corresponds to $\frac{1}{150 \text{ MHz}} = 6.67 \mu\text{s}$. The SSP detects if the signal from the SiPM shifts away from its baseline value. If this shift was above the trigger threshold, it registered an event, and digitized the event for output. The threshold chosen for these tests changed over time, but an ideal threshold was typically between 10 and 15 ADC counts.² The SSP converted the output into useful values, and output these as a 48-Byte encoded

²Refer to Section 4.3 for how this threshold was determined.

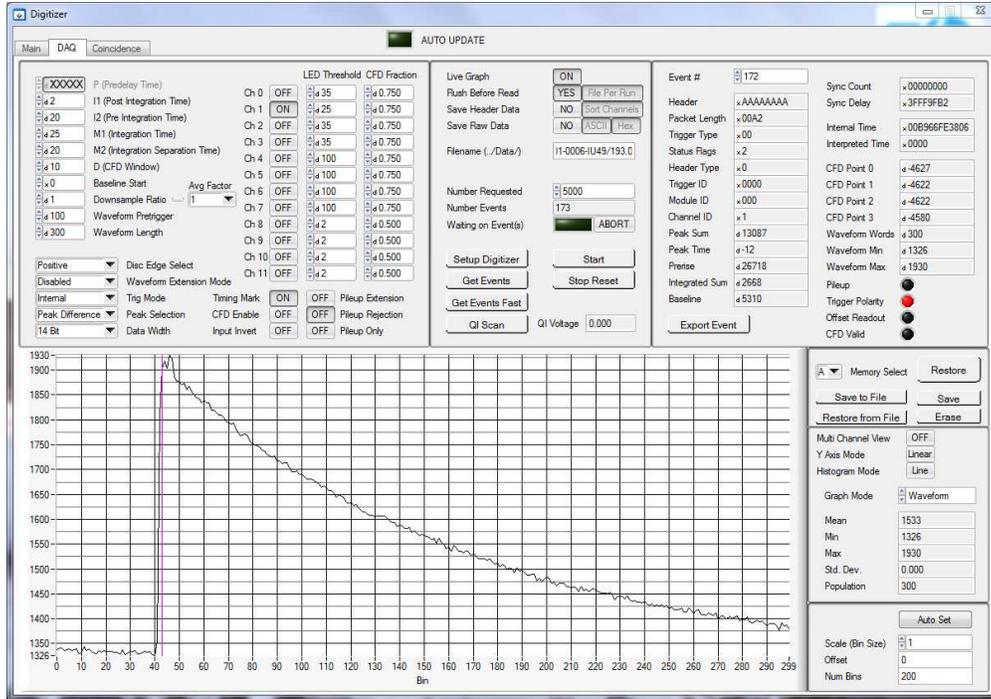
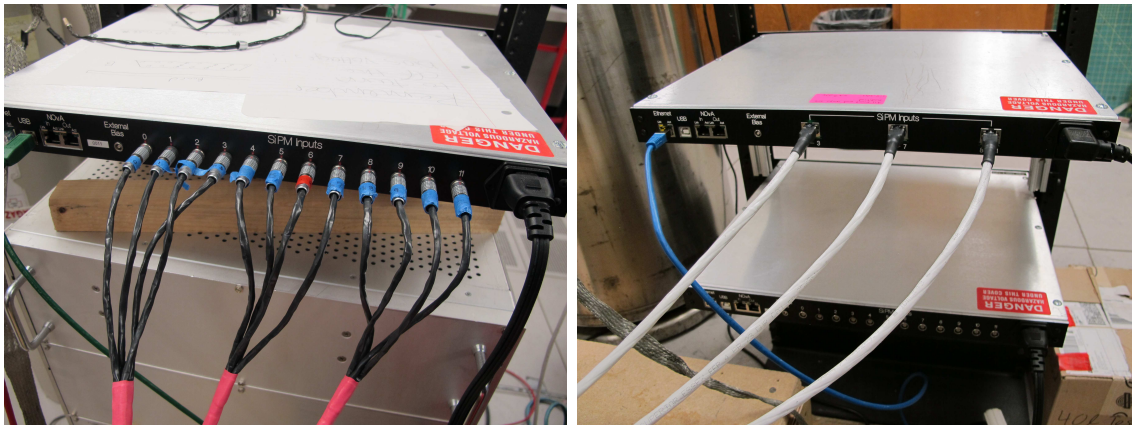


FIGURE 3.7. Single waveform output for a single PE event. The SSP has a 150 MHz clock, so 1 unit on the x-axis corresponds to $6.67 \mu\text{s}$. The y-axis is in ADC units, which has a conversion of $6.60 \times 10^{-3} \text{ mV} / \text{ADC}$.



(A) Early version SSP with twelve quadrapus (B) Newer version SSP with three RJ45 connectors, each corresponding to four channels.

FIGURE 3.8. This shows the two SiPM connection schemes. The newer SSP can take direct RJ45 connections, while the older version took quadrapus cables, which split the RJ45 connectors into the 4 individual channels.

packet, followed by the event waveform. A single event waveform resembled the example shown in Figure 3.7.

The event packet contained the channel ID for the event, a timestamp of the event, the baseline sum, the peak sum, as well as several other values describing the event. Only two critical pieces of information were needed to describe the event: the pulse amplitude and the integrated charge. The pulse amplitude described the maximum height of the pulse away from baseline. This was calculated by subtracting the baseline voltage from the voltage at the peak of the pulse. The integrated charge described the total charge deposited by the event. The integrated deposited voltage is calculated by taking the total integrated voltage and subtracting the integrated background. The units for this are based on discrete counts from the analog to digital converter (ADC). These can be directly converted to a voltage by a conversion factor of $1\text{ADC Count} = 6.60 \times 10^{-6} \text{ V}$ [22]. Once this is done, the total deposited charge must then be determined. This conversion from integrated voltage S to charge Q was calculated is given in Equation 1, as determined in reference [22].

$$(1) \quad Q = S \times \frac{6.60\text{V}/\text{ADC Count}}{100\Omega} \times 6.67 \times 10^{-9}\text{s} \times 10^{12}\frac{\text{pC}}{\text{C}}$$

The SSP has many configuration options, and for these studies the settings shown in Table 3.2. Refer to the SSP manual for a full description of these settings and what they affect[1]. The bias voltage provided by the SSP has an allowed range of 0-30 V. SiPMs must have an applied voltage greater than their breakdown voltage to function. If the applied voltage is greater than the breakdown voltage, this difference is called the overvoltage. The behavior of the SiPMs strongly depends on the overvoltage, and the pulse amplitude and integrated charge of events would change significantly by changing this value. The breakdown voltage ($V_{breakdown}$) of these SiPMs has a significant temperature dependence. This is around

25 V at room temperature, and around 20 V at LN2 temperature. These tests were all performed at 25.5 V applied bias, which should provide a relatively large and constant overvoltage. The full reasons for using the voltage are described in Section 4.3.

SSP Parameter	Setting
Constant fraction discriminator bit field	0x1800
Readout window (# of 6.667 ns samples)	350
Readout trigger	100
P Window (delay between external trigger and event)	2
i1 window (post trigger window)	500
m1 window (window for preRise and peakSum)	10
m2 window (rising window - from preRise to peak)	10
d window (post trigger window)	20
i2 window (pre trigger window)	500
Discriminator width for trigger output	10
Baseline start	0x0000
Channel control mode	0x90F00801
Default threshold	200

TABLE 3.2. SSP settings used in our testing. Full descriptions of these parameters are given in the SSP manual[1].

CHAPTER 4

EXPERIMENTAL RESULTS

Thermal cycle tests were performed over the period from July 2016 to January 2017. The procedure evolved over this time. For this study, an individual “test” is defined as all thermal cycles from when a CB was installed in the mounting assembly until it was removed, while a “run” is defined as a single session of biasing the SiPMs and recording event output. The underlying goal of this study was to qualify the SiPMs and readout boards for use in protoDUNE. There were a number of potential failure points in the SiPM system, most notably in the SiPM devices, the PCBs, the RJ45 connectors, or the solder connections. These parts have not been designed to operate at cryogenic temperatures. This study was to verify that the SiPMs and the designed readout board will function at cryogenic temperatures, even after repeated thermal shocks. The test procedure will be described, as well as various aspects of the testing which were improved over time. We will explain how the results of this testing were analyzed, and what results were found from the study. Before describing the test procedure, it is critical to understand the operating characteristics of the SiPMs.

4.1. SiPM CHARACTERISTICS

For this study, it was necessary to quantitatively describe some of the operating characteristics of the SiPMs. These parameters can be evaluated after each thermal cycle to determine changes as a function of thermal cycle. The three main parameters examined in

this test sequence were the gain, dark rate, and crosstalk.¹ Dark rate and crosstalk were determined using the pulse amplitudes, while gain was determined using the integrated charge for events from the SiPMs. A plot of pulse amplitudes for a single run of an SiPM is shown in Figure 4.2a. The sharp peaks correspond to individual numbers of photo-electrons (PE); peaks are clearly defined corresponding to one PE, two PE, etc. An additional peak may sometimes appear left of the single photo-electron (PE) peak, which corresponds to noise in the system, or pedestal. A non-noisy cycle may not have this peak appear at all, while an especially noisy cycle may have this noise peak appear many times larger than the single PE peak. By varying the threshold of where to trigger events, we can lower this pedestal, or remove it entirely. This will be discussed in more detail in Section 4.3.

4.1.1. **GAIN.** The gain is a measure of the ratio of the total deposited charge to the light incident on the SiPM. For each run a histogram of the integrated charge is examined, and the charge of the peaks corresponding to one PE and two PE are determined. The charge difference between the centroids of these two peaks corresponds to the charge deposited by one PE. The reason to use this difference rather than the center of the one PE peak is to account for any offset that could appear in the integrated charge. The photon has no charge, but a PE does have the charge of a single electron (1.6×10^{-7} picoCoulombs). This is used as the incident charge on the detector. The gain is calculated by taking the ratio of this charge difference to the electron charge, as shown in equation 2[22].

The gain of each channel on every run was determined by:

$$(2) \quad G = \frac{\langle q_{2pe} \rangle - \langle q_{1pe} \rangle}{q_e}$$

¹The rate of after-pulsing is another characteristic of interest, but due to technical constraints it is not examined in this study.

where G is the gain, $\langle q_{2pe} \rangle - \langle q_{1pe} \rangle$ is the total deposited charge, and q_e is the electron charge.

4.1.2. **DARK RATE.** The dark rate is the rate of single PE noise events the SiPMs observed with no scintillation. These events can be created by thermal excitations, and thus the rate depends on temperature and overvoltage. At the boiling temperature of liquid argon (87 K), a typical dark rate for these devices is around 10 Hz. Since liquid nitrogen has a boiling temperature of 77 K, its dark rate is comparable. We calculate the dark rate by integrating the total number of events with pulse amplitude $^{1/2}$ PE and above, and dividing by the total runtime.

The dark rate of each channel on each run was determined by:

$$(3) \quad R_D = \frac{\sum x_{\geq 0.5pe}}{t_{run}}$$

where R_D is the dark rate, $x_{\geq 0.5pe}$ is the measured pulse height for events above $^{1/2}$ photoelectrons, and t_{run} is the total runtime.

4.1.3. **CROSSTALK.** Crosstalk describes how one avalanche on an SiPM cell, or pixel, can induce a second avalanche on the same SiPM at a different pixel. Since our expected dark rate is 10 Hz, and the readout window is order of microseconds, the probability of two dark events occurring at the same time is negligible[22]. Therefore, any events with energy greater than 1PE in amplitude are likely caused by crosstalk, not multiple dark events. The crosstalk is defined as the ratio between these multi-avalanche events over the total number of photon events. To account for noise in the electronics (not due to dark counts), the calculation for this is done by taking the ratio of events with energy greater than 1PE divided by the total

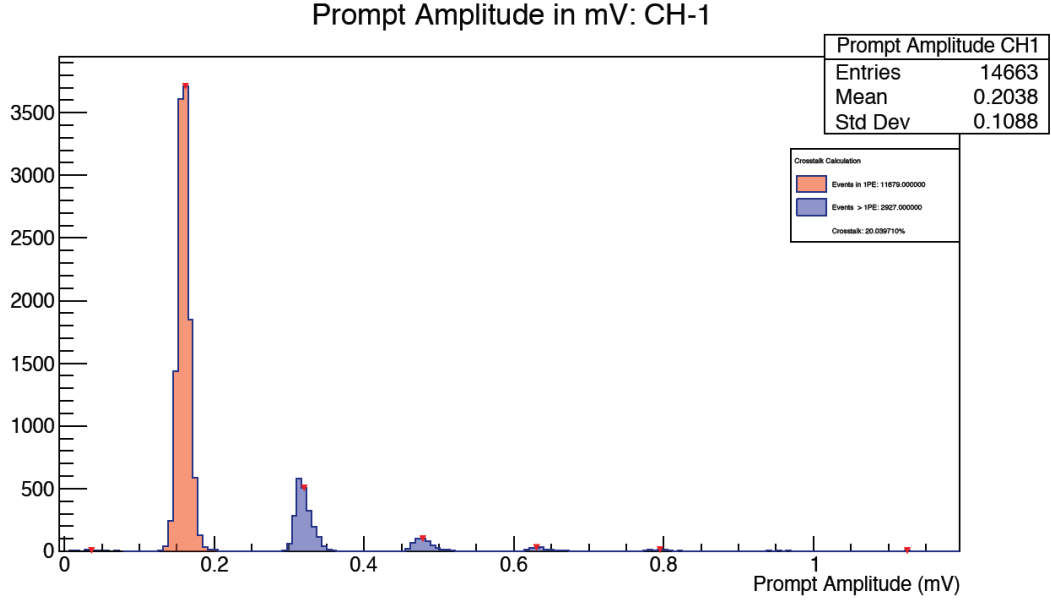


FIGURE 4.1. Plot of pulse amplitudes, showing 1PE events (red) and events from greater than 1PE (blue).

PE events. The cutoffs for this are chosen such that the left edge of the 1PE peak is 0.5PE, and the right edge is 1.5PE. The expected value for this crosstalk should be around 20% for the SiPMs we are testing based on previous testing[22].

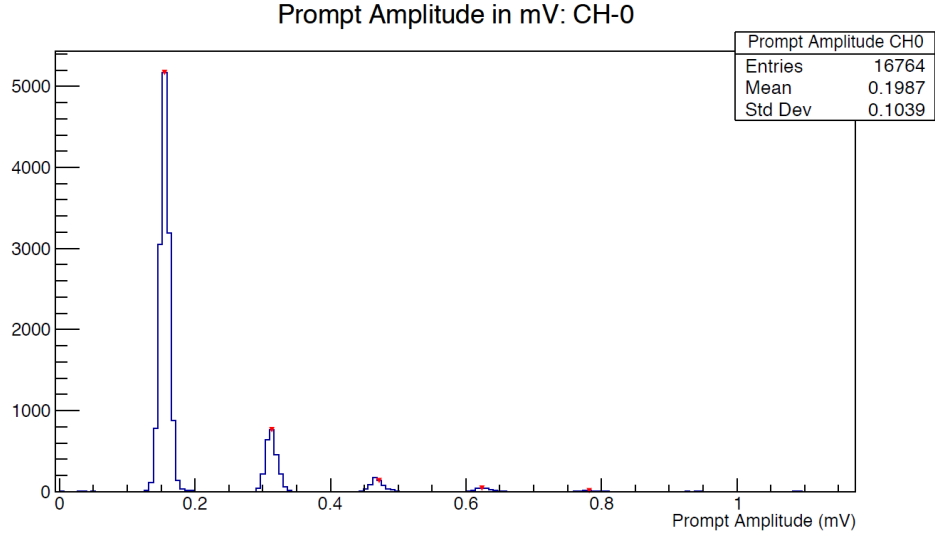
The crosstalk for each channel on every run was determined by:

$$(4) \quad C = \frac{\sum x_{\geq 1.5pe}}{\sum x_{>=0.5pe}}$$

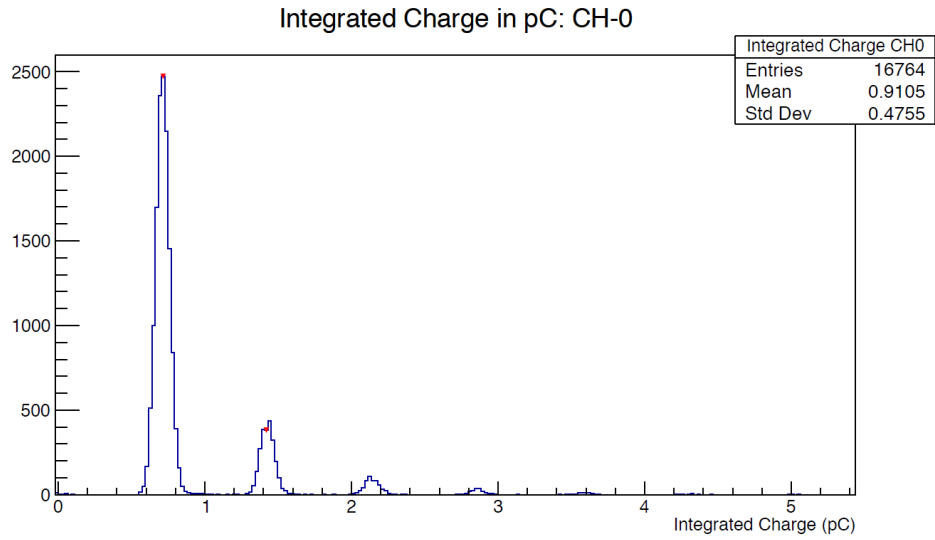
where C is the crosstalk, $\sum x_{\geq 1.5pe}$ is the number of events above $1\frac{1}{2}$ photoelectrons, and $\sum x_{>=0.5pe}$ is the number of events above $\frac{1}{2}$ photoelectrons.

4.2. TEST PROCEDURES

To study changes caused by thermal cycling, the boards had to be characterized before entering the cryogen. Each board underwent a pre-test to check for basic operation before it was installed for a test. Each test involved at least one thermal cycle. The results of



(A) Pulse Amplitudes



(B) Integrated Charges

FIGURE 4.2. Histograms for the pulse amplitude and integrated charge. Clear peaks are visible corresponding to 1PE, 2PE, etc.

these tests were thoroughly examined, and any possible signs of SiPM or board failure were investigated. A list of these is shown in Table A.2.

4.2.1. FABRICATION AND PRE-TEST. The fabrication of the test boards used both local and third party resources. As discussed in Section 3.1, the PCBs for the test boards were

designed at CSU, but manufactured at Advanced Circuits in Fort Collins, CO. The SiPMs were placed on the PCBs at CSU, and the process is fully described in Ref. [21].

Once fabricated, a visual pre-test was performed to ensure no visual defects were observed in either the SiPMs or solder connections. A photograph was taken of the board, as well as a magnified photo of each individual SiPM, as shown in Figure 4.3. This image included the area around the SiPMs to look for defects in the proximity, and at the solder connections. The boards were then tested at room temperature in a dark box. An ultraviolet LED was pulsed to provide distinct non-noise photons to test operation before undergoing any thermal cycles.

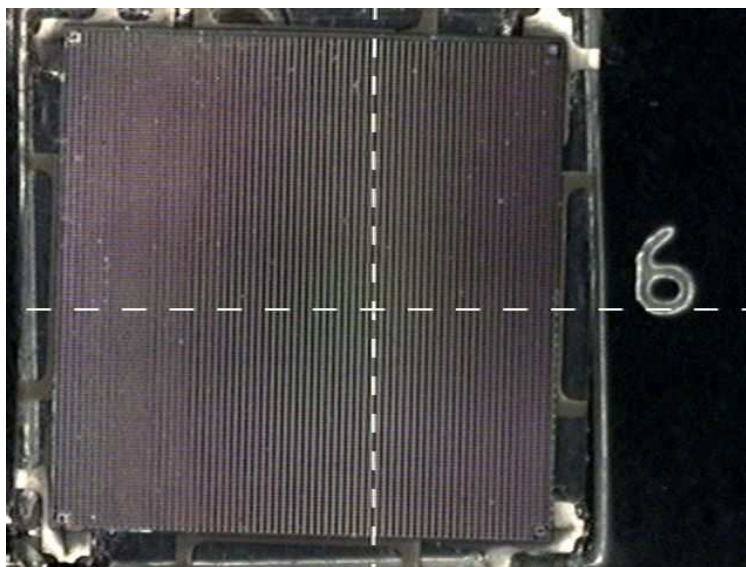


FIGURE 4.3. Example closeup photograph taken of an SiPM before thermally cycling.

4.2.2. PREPARATION OF TEST APPARATUS. For DUNE, it is possible that some readout boards will need to be replaced over the course of operation. However, it is unlikely a board will need to be reinstalled. For this study, previously tested boards were looked at multiple times to either put them through more thermal cycles, or to more closely examine any peculiar behavior that was observed. Once the CB was installed for a test, a diode

measurement was taken to ensure a complete circuit and to ensure proper diode behavior of the SiPM. This helped to ensure no solder connections were damaged during install and that the SiPM was functioning. Every CB installation and removal is listed in Appendix A. This helps to determine if there are any issues which appear during an individual installation.

Before the test boards could be lowered, the dewar was filled with LN2. The light box was closed tightly, which helped prevent extra air from entering. Filling the LN2 cools off the dewar very quickly, and in the process evaporates a large amount of the LN2. This flooded the dark box with nitrogen gas, preventing frost from forming. The depth of the tank was monitored during the fill by a capacitance meter to prevent overflow. Once it was filled, the test mount containing the boards was slowly lowered into the nitrogen at a constant rate, taking around 30 minutes. Once the mount was all the way down and the top of the dewar sealed, the system was ready for testing. After data for the cycle was taken on all boards, or at the end of the day, the mounting system was raised, again taking around 30 minutes. Before, during, and for an hour after the raising, gaseous nitrogen was flowed through the dark box again to prevent frost formation. During this hour, the system returned to room temperature, and the nitrogen gas flow was turned off. As previously mentioned, any number of cycles could be performed following this single installation. However, the LN2 evaporated over time, and the dewar had to be topped off with LN2 every day to ensure the CBs were fully submerged. After the tests, the boards were uninstalled, and stored in anti-static bags away from the light.

4.3. TESTING STRATEGY

The test results are highly dependent on initial settings, such as bias voltage or trigger threshold. These had to be determined before the study, and kept constant throughout.

Other variables such as runtime should not effect SiPM characteristics, but should also be constant to keep sufficient and consistent statistics. Gain is proportional to overvoltage: $G \propto V_{Overvoltage} = V_{Applied} - V_{Breakdown}$, so a small change in the applied voltage could measurably change the gain. The breakdown voltage of the SensL SiPMs is around 21 V while submerged in LN2 based on testing by other groups[23]. The chosen applied voltage of 25.5 V was well past breakdown voltage, but not high enough to cause damage to the SiPMs or cause high noise. For reference, the recommended overvoltage is 1.0-5.0 V, so the voltage used is right at the maximum recommended by SensL[20]. Additionally, other groups using these devices are using this 25.5 V bias voltage, making it simpler to compare the results among similar studies. As such, 25.5 V was applied for all tests in this study.

Another important determination made for this testing was the threshold. Unlike for gain, the threshold can be slightly changed between cycles without affecting the measured SiPM characteristics. The threshold defines what the SSP should count as an event for our data, where only pulse amplitudes higher than the threshold were counted. By setting an appropriate threshold, most noise will not trigger as an event, and noise will be largely removed. However, if the threshold setting is too high, then PE dark counts will no longer register. A reasonable choice of threshold is $\frac{1}{2}$ PE, which cuts off most noise while cutting well before the 1PE peak. While the characteristics and the 1PE peak will vary with bias voltage, at a constant 25.5 V bias this peak should remain relatively consistent in pulse amplitude for all SiPMs. These characteristics may vary slightly from one SiPM to another, but the individual devices should all be consistent. The determination of threshold values is illustrated in Figure 4.4. This plot shows the number of triggered events from an SiPM as a function of the threshold. The runs were performed consecutively, increasing the threshold

by 1ADC at a time beginning at 15ADC. The total number of events start flat, begin to fall at the leading edge of the 1PE peak, and then flatten out again at the trailing edge of 1PE. The dropoff in events is due to the threshold starting to cut into 1PE events, and dark count events going undetected. Since valid events are lost, the dark rate, crosstalk, and gain calculations were inaccurate for such runs. This study demonstrated that the dropoff was observed just after a threshold of 20ADC, as seen in Figure 4.4. Any threshold above 20ADC will result in inaccurate parameter calculations, so data taken from channels while threshold is above this are disregarded in our testing.

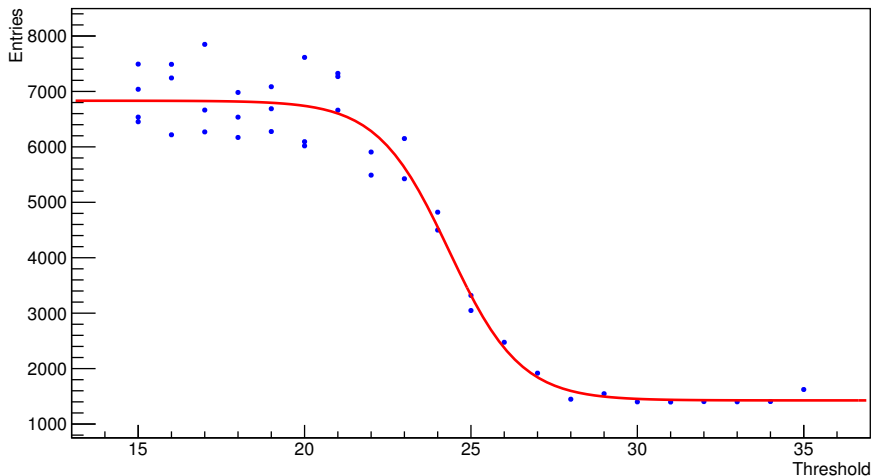


FIGURE 4.4. Total number of triggered events from an SiPM as a function of the threshold. The observed drop in events is due to the threshold cutting into the 1PE peak, where the beginning and end of the drop correspond respectively to the leading and trailing edge of the 1PE peak. The x-axis of this plot is in ADC, which can be directly converted to voltage by the conversion:
 $1\text{ADC} = 6.60\mu\text{V}$.

While gain, dark rate, and crosstalk should be independent of runtime, varying runtime will change the number of events which effects the statistics of the study. Since the uncertainty in the values depends on N, longer runtimes should provide lower percent statistical uncertainty. It was more efficient to have a full four boards installed at once due to the time

requirements for a test. The three boards not being tested were left entirely disconnected to the rest of the testing system, which served to keep each run entirely independent of the other boards installed in the cold tester. The process used was to fill the dewar and lower the mount, and then connect the Cat6A cables to one of the boards. Data were taken on this board, and then the Cat6A cables were disconnected and moved over to the second board, without raising the mount. In this manner, data were taken on all four boards one after the other, only requiring one lowering of the mount. This process is shown in Figure 4.5, which outlines the procedures used on the boards from fabrication, to testing, to storage. A runtime of 1200 s (20 minutes) was chosen for these experiments, which at an expected dark rate of ~ 10 Hz/Channel, gives an expected ~ 10000 events/cycle. These 10000 events should give statistical uncertainty of $\sigma_{stats} = \frac{1}{\sqrt{N}} = 1\%$. Using 1200s runs then should provide statistics slightly better than 1%, while also being a convenient number to use for our calculations. A set of four boards could be tested at this runtime in less than two hours, even while allowing 10 minutes in between boards for cabling and setup. This allowed for the possibility to perform two cycles for four boards in one day, with sufficient time for lowering or raising the mount, and replacing the four installed boards with a new set of four boards.

4.4. TEST ANALYSIS

A total of 63 CBs were tested, corresponding to 756 SiPMs. See Table A.1 for a full list of these boards, and the number of thermal cycles they underwent. The tests were ended for a several different reasons. Most boards were tested for a predetermined 5 cycles, but some warranted further study. A few boards were tested for much more, up to 30 cycles. Different boards underwent varying number of thermal cycles, for several reasons. Some

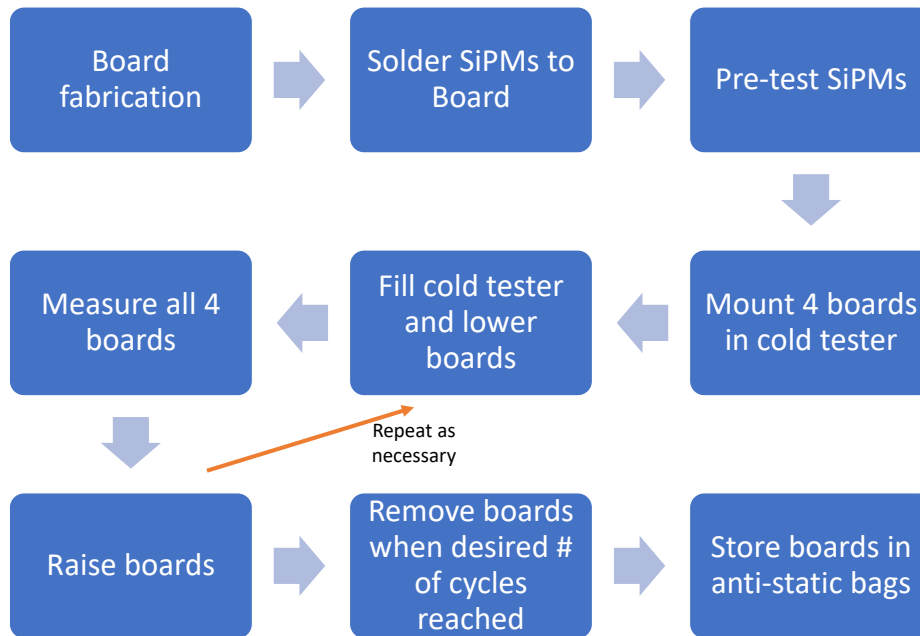


FIGURE 4.5. Flow chart of procedures used for boards.

boards showed unexpected behavior and needed more detailed testing, such as some boards showing “ringing” in their waveforms.

The analysis for this study was done by first determining the SiPM parameters of single runs, and then examining the change in parameters over multiple runs. A program known as ROOT is used for both steps of the analysis[24]. This program was developed at CERN, and is used throughout HEP research. As shown in Figure 4.2a and Figure 4.2b, the events cluster into Gaussian distributions. The peak locations of these Gaussian distributions are determined using ROOT’s `TSpectrum` class, which searches for peaks in the raw data. Parts of the search function can be changed, such as allowed variance (σ) of the peak and minimum peak threshold from maximum. These peaks are then fit to a series of Gaussian functions, in order to determine the peak height, width, and central value. The fits were performed using the `TH1` class’ “Fit” function in ROOT. Examples of such fits are shown in Figure 4.6 and

Figure 4.7. Noise peaks, determined by peaks below 0.5PE, are not fit to Gaussian functions or used in calculations.

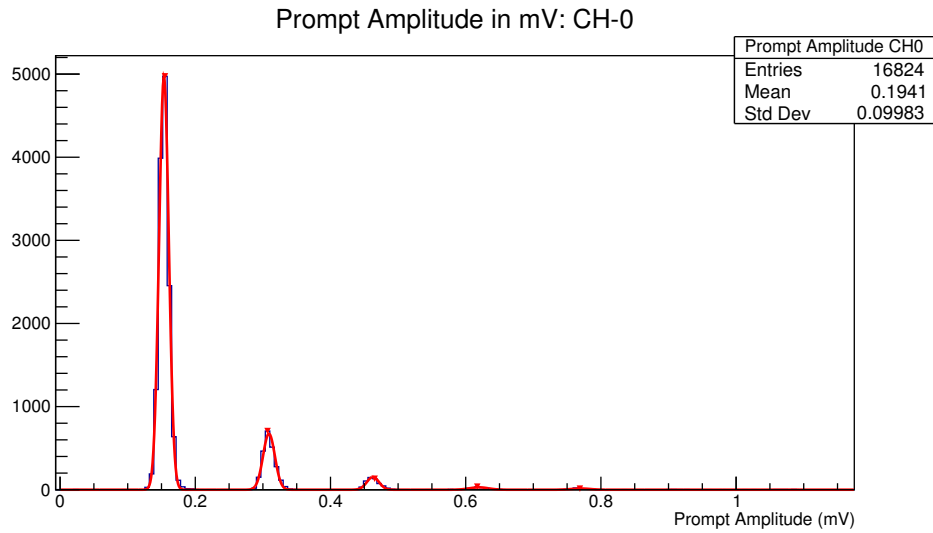


FIGURE 4.6. A pulse amplitude histogram, with peak locations and fits shown in red.

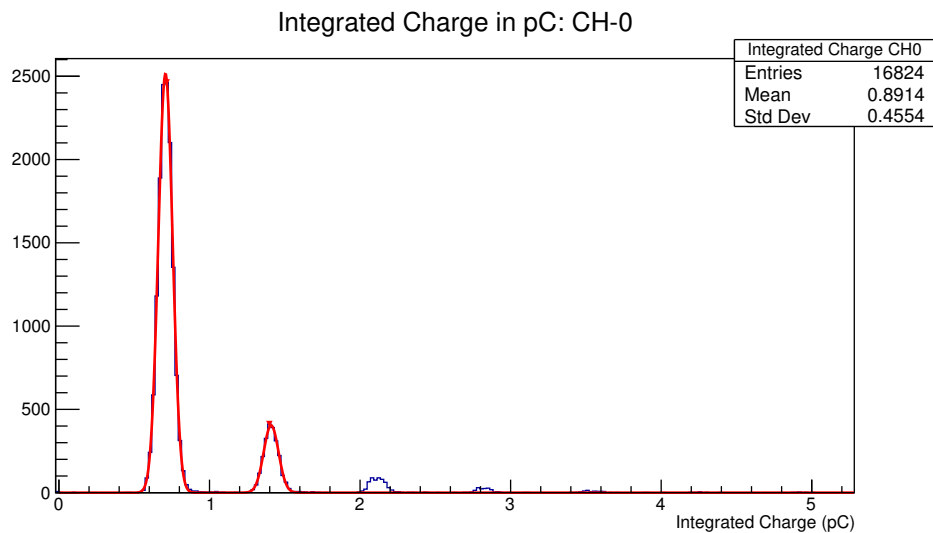


FIGURE 4.7. An integrated charge histogram, with two peak locations and fits shown in red.

Once the peak information was determined, calculations were performed to determine the gain, dark rate, and crosstalk. All data and analysis quantities including histograms, pulse waveforms, fits, calculated characteristics, were stored in a single file for easy access. Once

this analysis had been performed on all boards, the results were analyzed for all cycles. A python script was written to collect all analyses data, and combines all of their information into a convenient data structure. Each parameter was plotted against thermal cycle for each test board in the study. An example of such is shown in Figure 4.8, with each symbol representing a different channel. The full list of these for all boards is shown in Appendix C.

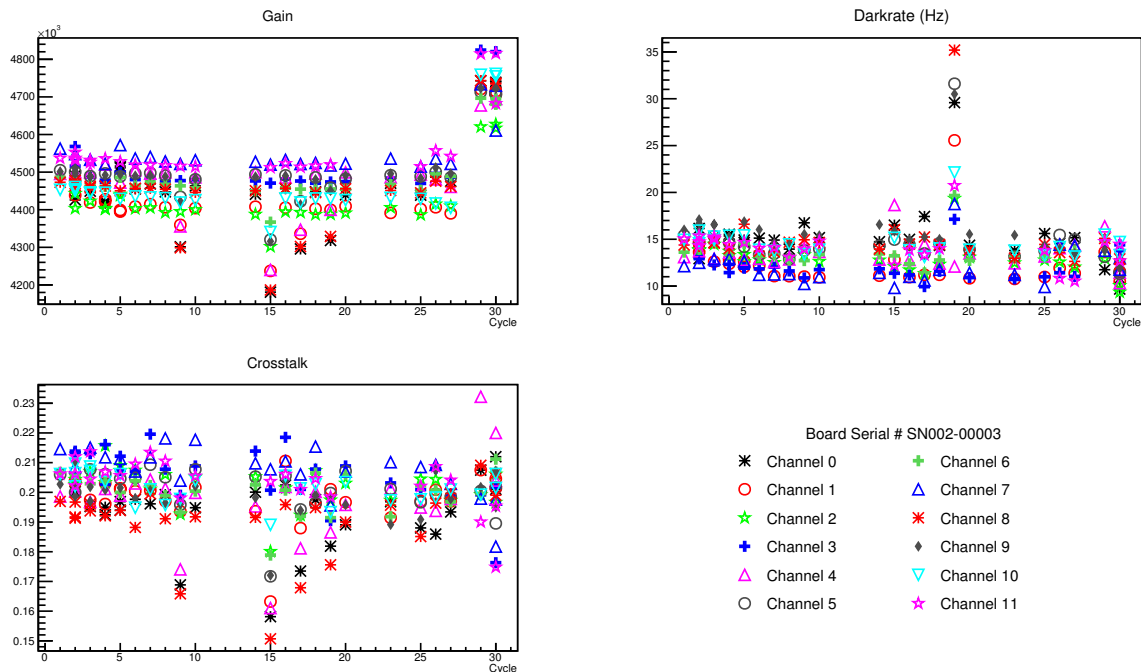


FIGURE 4.8. Thermal cycle analysis for cycle board SN002-00003. The gain, dark rate, and crosstalk have been plotted for each of the 12 SiPM channels.

4.5. RESULTS

To determine whether or not there was evidence of thermal damage, we examined the plots of gain, dark rate, and crosstalk versus cycle for each board and channel (SiPM). For each of the plots of SiPM parameters (as shown in Figure 4.8), we check that the device parameters are consistent without systematic drift, and that they are close to the expected values.² Each of these plots was examined by hand and observed irregularities were further

²Expected gain: 4×10^6 , expected dark rate: ~ 10 Hz, expected crosstalk: 20%.

studied. The process for this is outlined in Figure 4.11. If the cause of the irregularity could be satisfactorily explained as something other than thermal damage, the data were removed from the plot. Some causes of these irregularities were as follows; high noise in the data (which could include electronic “ringing” in the waveforms), a high rate of PE events (over 10^6 compared to the expected value of $\sim 10^4$), or less than half the expected number of events (below 5000 compared to $\sim 10^4$). Figure 4.9 plots the waveforms resulting from electronic ringing during a run, and shows how the noise surpasses the 1PE peak. As shown in Figure 4.10, this high noise overwhelms the data and prevents proper determination of PE peak information for parameter calculations. In the event of these well-understood irregularities, the results from such were removed from the thermal cycle plots. The full list of exclusions is given in Appendix B. In some cases, no run with a valid trigger threshold (20 or below) could finish without crashing the readout code. And in other cases, run data were not able to be taken on every board during a thermal cycle. All of these lead to empty channels in the thermal cycle plots. This shows that even though run data were unavailable, the devices underwent a thermal cycle.

Additionally, occasional “jumps” occurred to all channels from one cycle to the next. One cause of this was the replacement of the SSP, as shown in the increase of the gain for cycles 29-30 in Figure 4.8. While the two SSPs are claimed to operate identically, all boards which were tested on both boards show a sudden increase in gain once the SSP is swapped. Similar jumps showed up elsewhere as well, however, not corresponding to changing the SSP, and were transient. Peculiarly, these jumps oftentimes will occur for only one cycle, and then the following cycle all values will return to their initial values. Many of these could be accounted for when more closely examined. These jumps were often due to higher noise in the system

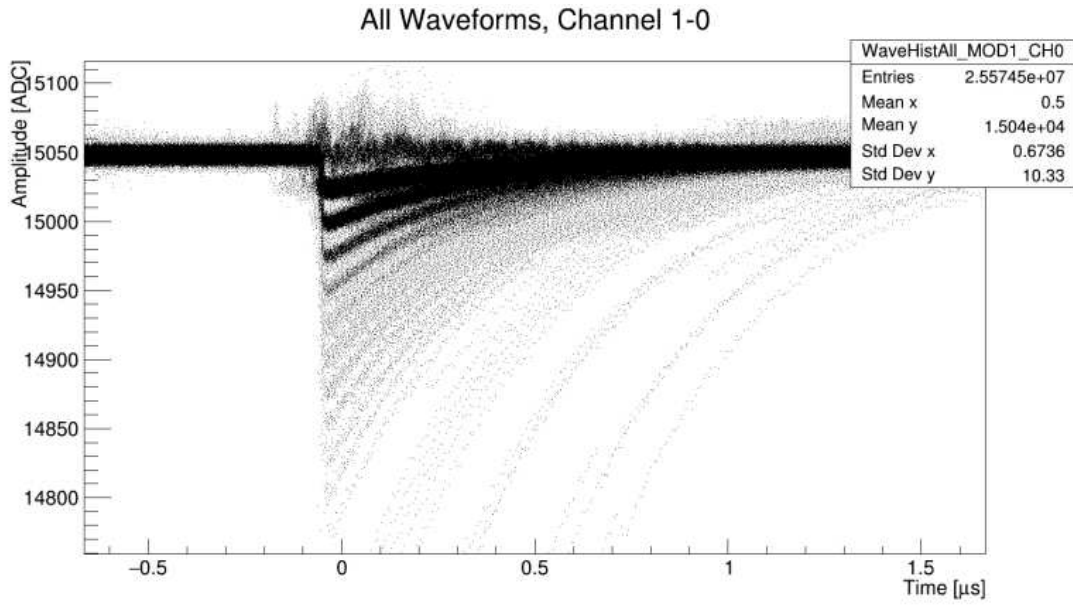


FIGURE 4.9. Example of high noise due to electronic “ringing” in the test system. Note that raising the threshold to remove the ringing would also remove events in the 1PE peak.

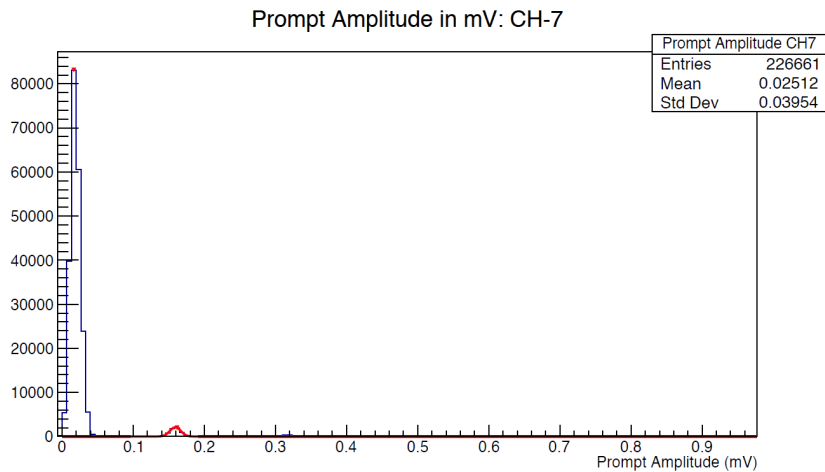


FIGURE 4.10. Example of high noise (the first peak) oversaturating the data, such that the PE peaks cannot be easily identified. In this case, the 1PE peak is fit, but no higher PE peaks are able to be identified in the data.

than usual interfering with the parameter calculations. Since these jumps happen to all channels at the same time, and will reappear and disappear from one cycle to the next, they do not seem to be evidence for thermal damage. These jumps in our data seem to be due to an issue in our setup, likely somewhere in the cabling of the cycle board to the SSP, but

this has not been thoroughly explained. For example, we have had issues with some of the RJ45 connectors which were not able to be fully addressed during the study.

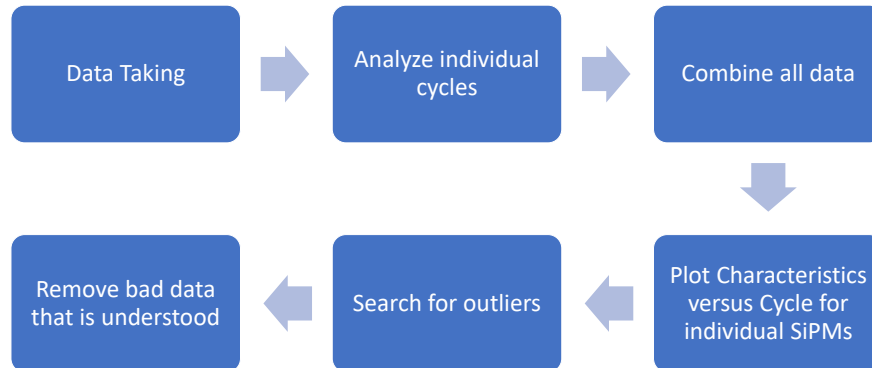


FIGURE 4.11. Flow chart of analysis procedure.

The number of cycles performed on boards in the study varied from 5 to as many as 30. The example in Figure 4.8 shows the results of one such long series of cycles, and exemplifies many common features of other CBs' final thermal cycle analyses. In this example, the readout board was cycled 30 times, but run data were only available for 23 thermal cycles. The most common reason to remove cycles was due to very high noise, on the order of several hundred Hz. A channel with high noise would have a drastically large pedestal peak before the 1PE peak. A noise peak that was too high would lead to difficulty in determining the locations of the PE peaks. Since the analysis calculations are done using peak locations, the high noise ended up swamping out the PE peak locations necessary for calculation.

Since most CBs had plots of parameters versus thermal cycle which looked much like Figure 4.8, this figure can help describe the general results. As predicted, the dark rate was around 10 Hz (closer to 15 Hz, and varied by board), the gain was around 4×10^6 , and the crosstalk was around 20%. The characteristics for these readout boards seem to maintain

quite well over a large number of thermal cycles, but cycles 15, 19, 29, and 30 show large fluctuations from nominal. These fluctuations seem to affect all SiPMs at once, however, and then disappear just as suddenly in following runs. This is much more characteristic of a problem with the testing setup for that cycle as opposed to problems in the SiPMs. Some causes of these problems could be cabling issues, power fluctuations in the SSPs, or poor contact with the RJ45 connectors. In some other boards, there is a sudden shift in all values. These were found to correspond to exactly when the new SSP replaced the old one. In these cases, it is likely the two SSPs were not calibrated to the same voltage. The 25.5 V provided by the new SSP may not be the same voltage provided by the old SSP at 25.5 V. We were unfortunately unable to confirm this, since neither SSP design provides an output for voltage calibration. Further studies could be done to determine whether or not this is the case, such as designing a system to connect the LEMO and RJ45 connectors on the SSPs to high voltage measurement equipment. Other than these overall board fluctuations, parameters were very consistent.

There is one unexplained phenomenon in our results which initially seemed to show signs of thermal damage. Figure C.9 shows a drift in SiPM parameters in board SN00300007 for cycles 22 and 23. This drift seems to have increased over thermal cycles, which is consistent with a mechanical failure worsening over more cycles. However, this same shift occurs for the same thermal cycles in board SN00300009, as shown in Figure C.11. While it is possible for a whole board to fail simultaneously (due to failures in the solder or connections), it is not reasonable to assume that two boards failed during the same cycles in exactly the same way. Moreover, a further test of SN00300009 showed a return to nominal values (except for an increase in gain due to switching to the upgraded SSP). This implies that the fluctuation was

due to problems in the testing system, not due to failures in the SiPMs or readout boards. The cause of the fluctuation was never determined, and further testing of these devices would be beneficial to determine what part of the test system was responsible for this behavior. Other than these cycles for these two boards, there were no obvious permanent changes in these parameters due to thermal cycling. The thermal cycling process showed no signs of SiPM or board failure no-matter how many cycles were performed.

4.6. TESTING IMPROVEMENTS AND ISSUES

The test procedure was modified over the course of these studies for a few reasons. One major change was the replacement of the SSP partway through testing. The original quadrapus design used between September 9th and October 4th only had two quadrapus cables available for testing. Two 1200 second runs had to be done for a single board in these tests. An initial run recorded data on channels 0-7, while channels 8-11 remained disconnected. After this run finished, a second was performed on the same board without raising boards out of the LN2. This run recorded the data on channels 4-11, while keeping channels 0-3 disconnected. These two runs together gave data for every channel of the board for the same thermal cycle. The extra data on the channels 4-7 (used on both tests) were kept, and show up in our analysis for these boards. The upgraded SSP no longer required these quadrapus cables, and instead used custom Cat6A cables with regular RJ45 connectors to read each cable directly, and split the channels internally.

After testing had begun, a critical issue arose which prevented further detailed testing. The full thermal cycle analysis had yet to be completed, but no glaring issues had appeared, especially none which seemed to indicate thermal damage. Midway through the testing, mechanical failures began occurring on a large percentage of a newer batch of SensL SiPMs.

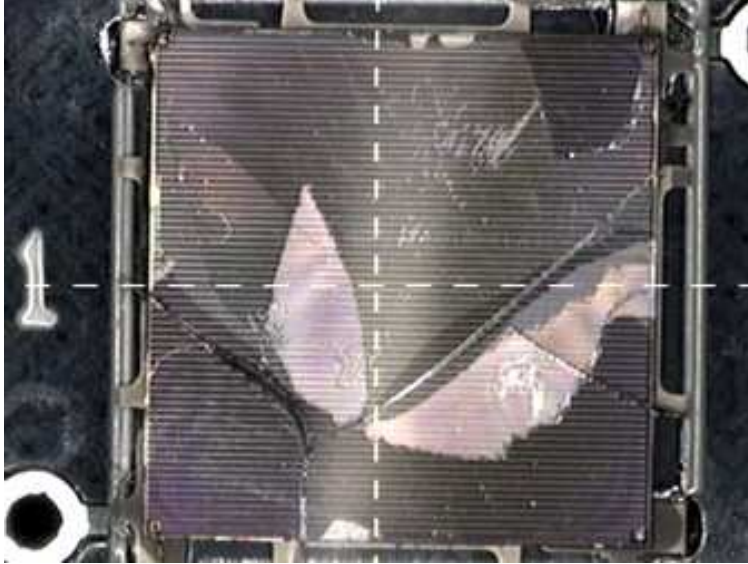


FIGURE 4.12. Close up image showing a SensL C-revision SiPM suffering thermal damage after being immersed in LN2.

Such failures were clearly visible by eye, and an example of such a failure is shown in Figure 4.12. It was unknown at the time whether the failures were the result of a change in the SiPMs, or an issue related to the the solder or other interface between the SiPMs and the readout boards. In order to determine whether a change in the SiPMs had caused this failure, a procedure was implemented to thermally cycle six SiPMs which had yet to be mounted to a readout board. If the same failure was seen in this test, the fault was likely due to the SiPMs themselves rather than another part of the readout board. This test placed the six SiPMs into a metal mesh basket, which was lowered into the LN2 at the same rate as the other thermal cycle tests.

When the basket containing the SiPMs first entered the LN2, a popping sound was heard. Three of the six SiPMs experienced the mechanical failures seen on the readout boards. This test showed that the SiPMs themselves were failing when entering the LN2, and at a high rate ($\sim 50\%$). We contacted SensL directly to find out if they could provide any insight into this problem. SensL confirmed a minor change had been made in the SiPM packaging. The

only change easily noticeable for consumers was a different nomenclature system for the serial numbers on the SiPMs. The SiPMs produced before this change are referred to as A-revision, and the ones produced after are referred to as C-revision. These newer C-revision SiPMs seem to have a near 50% rate of this catastrophic failure resulting from thermal cycling, and are not ideal photosensors for use in LN2 or LAr.

The SensL SiPMs will still instrument the protoDUNE photon detection system. The design of protoDUNE intended for 720 of these detectors to be used in the photon detection system. Only 540 of the A-revision devices remained available, meaning they must be handled with care. The initial plan on SiPM testing had to be revised to lower potential risk to these devices. The individual A-revision SiPMs destined for protoDUNE will be given only minimal testing; merely one thermal cycle each to verify they operate within expected parameters. Given the results in this thesis, we are confident that the SiPMs can be verified for thermal cycling in this way. In addition to these A-revision devices, C-revision devices will be used in protoDUNE as well. The failure rate of the C-revision devices is lowered after they are soldered onto readout boards. Our testing indicates approximately $\frac{1}{2}$ of readout boards with C-revision SiPMs will have a failure. All A-revision SiPMs readily available will be used in the photon detection system, while the remaining SiPMs used in the photon detection system will be the C-revision devices. The expected failure of these devices means that without increasing the number of SiPMs used, there will be efficiency lost in the photon detection system. The results from the protoDUNE experiment will still play an important role in determining designs for the photon detection system for DUNE.

CHAPTER 5

CONCLUSIONS

The photon detection system is a critical component to protoDUNE. The photosensors have yet to be decided upon, however. SensL SiPMs seem like appealing photosensors for several reasons, including their compactness, their lower voltage requirements to PMTs, as well as their relative cheapness. However, these devices are not rated for cryogenic temperatures. This study sought to determine how these devices functioned at cryogenic temperatures, and to see if they are damaged by the large thermal shock which occurs when entering or leaving cryogenic liquid. We chose to perform this study using LN2 rather than LAr, since it prevents events which would occur from cosmic rays, it is cheaper than LAr, and the thermal shock from it is at least as large as it would be using LAr.

This study examined 150 C-series SensL SiPMs and corresponding mounting boards. The characteristics used to describe the performance of the SiPMs were their gain, dark rate, and crosstalk. The gain we observed using these devices was 4.4×10^6 , the observed dark rate was approximately 15 Hz, and the crosstalk was around 20%. It was found that these characteristics remain constant even after many thermal cycles. The SiPMs and mounting boards seem to work very well through thermal cycling, and there is no evidence for SiPMs being damaged by the cycling. There were several cases of cycles with individual SiPMs behaving poorly, but closer examination showed these issues to likely be the fault of the testing system, not of the SiPMs themselves. For example, electronic ringing in the system would result in seemingly nonsense results due to high noise, but these are consistent with a problem in the electronics of the test system, not of damage to the SiPMs. Other cycles showed jumps occurring to all SiPMs simultaneously, and then returning back to normal in

the next few thermal cycles. The revision change made by SensL left only a few of these SiPMs available for testing. SiPMs from after this minor change do show thermal damage from the cycling process. Only a small number of the original A-revision SensL SiPMs are available for testing, so they must be managed with care. The photon detection system in protoDUNE will utilize as many of the A-revision SensL SiPMs as are available. The newer revision of SiPMs from SensL will be used in protoDUNE, while taking into account that somewhere around 50% of them will likely fail due to thermal damage. Our study has shown that beyond the failure of these specific SiPMs, we do not expect any other significant cause of failure.

Despite initial difficulties in the testing system, and despite manufacturing changes making the intended devices obsolete, the testing system was shown to be very useful. If no more of the original devices are available, and the newer revision devices do not work, a next step would be to find a different model of SiPM that has similar operating capabilities. A few such devices have been suggested as alternatives, including SiPMs manufactured by Hamamatsu and FBK. The testing protocol would be relatively simple to perform on such devices, with the only considerable changes being how these new devices are connected to the SSP. In the event none of these SiPM devices work, there is also the option of resorting to a PMT-based photon detection system. Such a system has not been designed yet, but PMTs are known to be reliable photosensors. Determining the best photosensor for the photon detection system is a logical next step to DUNE, and the results of protoDUNE will provide much needed data about the full photon detection system. This additional information on possible photosensors will be used to decide which models are used in DUNE, and as such

whichever model of photosensor will play a considerable role in the next step for particle physics.

BIBLIOGRAPHY

- [1] J. T. Anderson *et al.*, *SiPM Signal Processor User Manual*. Argonne National Laboratory, 2.07 ed., 2016.
- [2] “ArDM - Argon Dark Matter experiment.” <https://www.http://darkmatter.ethz.ch/>. Accessed: 10/27/2017.
- [3] Wikipedia, “Standard Model of Elementary Particles,” 2017. [Online; accessed August 28, 2017].
- [4] S. Hatakeyama *et al.*, “Measurement of the Flux and Zenith-Angle Distribution of Upward Through-Going Muons in Kamiokande II + III,” *Physical Review Letters*, vol. 81, September 1998.
- [5] L. Brown, “The Idea of the Neutrino,” *Physics Today*, vol. 31, September 1978.
- [6] C. L. Cowan, F. Reines, F. B. Harrison, H. W. Kruse, and A. D. McGuire, “Detection of the Free Neutrino: a Confirmation,” *Science*, vol. 124, no. 3212, pp. 103–104, 1956.
- [7] B. T. Cleveland *et al.*, “Measurement of the Solar Electron Neutrino Flux with the Homestake Chlorine Detector,” *The Astrophysical Journal*, vol. 496, March 1998.
- [8] C. S. Wu, E. Ambler, R. W. Hayward, D. D. Hoppes, and R. P. Hudson, “Experimental Test of Parity Conservation in Beta Decay,” *Phys. Rev.*, vol. 105, pp. 1413–1415, Feb 1957.
- [9] J. H. Christenson, J. W. Cronin, V. L. Fitch, and R. Turlay, “Evidence for the 2π Decay of the K_2^0 Meson,” *Phys. Rev. Lett.*, vol. 13, pp. 138–140, Jul 1964.
- [10] A. Mirizzi *et al.*, “Supernova Neutrinos: Production, Oscillations and Detection,” *Riv. Nuovo Cim.*, vol. 39, no. 1-2, pp. 1–112, 2016.

- [11] M. Goodman, A. Heavey, A. Rubbia, and M. Thomson, “DUNE/LBNF CDR Volume 4: The DUNE Detectors at LBNF.” DUNE DocDB-183-v2: DUNE-doc-183-v2, 2016.
- [12] V. A. Kudryavtsev and DUNE Collaboration, “Underground Physics with DUNE,” *Journal of Physics: Conference Series*, vol. 718, no. 6, 2016.
- [13] D. Griffiths, *Introduction to Elementary Particles; 2nd, rev. edition*. Physics textbook, New York, NY: Wiley, 2008.
- [14] S. Fukuda *et al.*, “The Super-Kamiokande Detector,” *Nuclear Instruments and Methods in Physics Research Section A*, vol. 501, 2003.
- [15] D. S. Ayres *et al.*, “NOvA: Proposal to Build a 30 Kiloton Off-Axis Detector to Study $\nu_\mu \rightarrow \nu_e$ Oscillations in the NuMI Beamline,” 2004.
- [16] C. Rubbia, “The Liquid Argon Time Projection Chamber: A New Concept for Neutrino Detectors,” 1977.
- [17] T. Heindl *et al.*, “The scintillation of liquid argon,” *EPL (Europhysics Letters)*, vol. 91, no. 6, p. 62002, 2010.
- [18] X.-C. Lei *et al.*, “Evaluation of new Large Area PMT with High Quantum Efficiency,” *Chinese Physics C*, vol. 40, no. 2, 2016.
- [19] Hamamatsu, “Photomultiplier Tubes; Basics and Applications.” Handbook, 2007.
- [20] SensL, “C-Series Low Noise, Blue-Sensitive Silicon Photomultipliers: Datasheet.” Datasheet.
- [21] N. Buchanan *et al.*, “Quality Control Procedures for SiPM Mounting Boards.” DUNE DocDB-3773-v1: DUNE-doc-3773-v1, 2017.
- [22] D. Wittington, S. Mufson, and B. Howard, “Scintillation light from cosmic-ray muons in liquid argon,” *Journal of Instrumentation*, vol. 11, may 2016.

- [23] Y. Sun and J. Maricic, “SiPMs characterization and selection for the DUNE far detector photon detection system,” *Journal of Instrumentation*, vol. 11, no. 01, 2016.
- [24] R. Brun and F. Rademakers, “ROOT - An Object Oriented Data Analysis Framework,” *Nuclear Instruments and Methods in Physics Research Section A: Accelerators, Spectrometers, Detectors and Associated Equipment*, vol. 389, no. 1, pp. 81 – 86, 1997.
- New Computing Techniques in Physics Research V.

APPENDIX A

TESTED BOARDS

The following table (Table A.1) lists all boards tested during this thermal cycle study. Some of the boards were not used in the analysis, which are listed at the end of the table. Most of these were excluded due to not having enough thermal cycles. In the table shown, “Board SN” is a unique serial number shortened from identifiers on the PCBs provided by the manufacturer. The “Type” is either CB for cycle board, or HB for hoverboard. The “Date” is the date at which the board was manufactured. The Batch, Revision, and Cycles columns list respectively the SiPM batch, which revision of test board, and the total number of cycles performed.

Board SN	Type	Date	Batch	Revision	Cycles
072116-0005	CB	07-21-16	1	2	7
072116-0006	CB	07-21-16	1	2	5
080116-0007	CB	08-01-16	1	2	5
080116-0008	CB	08-01-16	1	2	5
001-00010	CB	01-19-17	2	3	1
002-00002	CB	08-31-16	1	3	29
002-00003	CB	08-31-16	1	3	30
002-00004	CB	09-07-16	1	3	12
002-00005	CB	09-07-16	1	3	5
002-00006	CB	09-07-16	1	3	8
002-00007	CB	09-20-16	1	3	2

Table A.1 – continued from previous page

Board SN	Type	Date	Batch	Revision	Cycles
002-00008	CB	09-20-16	1	3	30
002-00009	CB	09-20-16	1	3	18
002-00010	CB	09-20-16	1	3	28
003-00001	CB	09-20-16	1	3	11
003-00003	CB	09-20-16	1	3	18
003-00007	CB	10-03-16	1	3	24
003-00008	CB	10-03-16	1	3	26
003-00009	CB	11-01-16	1	3	25
003-00010	CB	11-01-16	1	3	2
004-00001	CB	01-19-17	2	3	1
004-00002	CB	01-19-17	2	3	1
004-00003	CB	01-19-17	2	3	1
004-00004	CB	01-19-17	2	3	2
004-00005	CB	01-19-17	2	3	1
004-00006	CB	01-19-17	2	3	2
004-00007	CB	01-19-17	2	3	2
004-00008	CB	01-19-17	2	3	2
003-0011	HB	11-02-16	2	2	32
003-0042	HB	11-02-16	2	2	32
004-0003	HB	01-12-17	2	2	1

Table A.1 – continued from previous page

Board SN	Type	Date	Batch	Revision	Cycles
002-0018	HB	01-12-17	2	2	1
004-0018	HB	01-19-17	2	2	1
003-0012	HB	01-20-17	2	2	1
003-00004	CB		1	3	7
003-00005	CB		1	3	10
003-00006	CB		1	3	12
063016-0001	CB	06-30-16	1	2	0
063016-0002	CB	06-30-16	1	2	0
071516-0003	CB	07-15-16	1	2	0
072116-0004	CB	07-21-16	1	2	0
002-00001	CB	08-31-16	1	3	0
003-00002	CB	09-20-16	1	3	0
004-00009	CB	01-19-17	2	3	0
005-00001	CB	01-19-17	2	3	0
005-00003	CB	01-19-17	2	3	0
002-00002	CB	08-31-16	3		
003-00004	CB		3		0
003-00005	CB		3		0
003-00006	CB		3		0
1	HB		1	1	0

Table A.1 – continued from previous page

Board SN	Type	Date	Batch	Revision	Cycles
2	HB		1	1	0
3	HB		1	1	0
4	HB		1	1	0
5	HB		1	1	0
6	HB		1	1	0
001-001	HB		1	2	0
001-002	HB		1	2	0
001-003	HB		1	2	0
001-004	HB		1	2	0
001-0018	HB	01-19-17	2	2	0
003-0036	HB	01-20-17	2	2	0
001-0008	HB	03-24-17	3	3	5
001-0010	HB	03-24-17	3	3	5
002-0016	HB	03-24-17	3	3	5
002-0010	HB	03-24-17	3	3	5
003-0032	HB	03-24-17	3	3	21
003-0042	HB	03-24-17	3	3	21
003-0046	HB	03-24-17	3	3	5
003-0017	HB	03-24-17	3	3	21
003-0020	HB	04-25-17	3	3	1

Table A.1 – continued from previous page

Board SN	Type	Date	Batch	Revision	Cycles
003-0064	HB	04-25-17	3	3	1

TABLE A.1. Devices tested for prototDUNE PD thermal qualification.

Board SN	Revision	Test #	Cycle	Reason for Ending Test
072116-0005	2	1	1-5	Predetermined number of cycles
072116-0005	2	2	6	Single test to examine re-soldered boards
072116-0005	2	3	7,8	Tests to study old vs new SSP
080116-0007	2	1	1-5	Predetermined number of cycles
080116-0008	2	1	1-5	Predetermined number of cycles
001-00010	3	1	1	Ended due to damaged SiPMs
002-00002	3	1	1-5	Predetermined number of cycles
002-00002	3	2	6	Ended to mitigate light leak
002-00002	3	3	7-26	Predetermined number of cycles
002-00002	3	4	27,28	Tests of board position in little dipper
002-00002	3	5	29	Ended to send board to ANL
002-00003	3	1	1-5	Predetermined number of cycles
002-00003	3	2	6-25	Predetermined number of cycles
002-00003	3	3	26,27	Tests of board position in little dipper
002-00004	3	1	1-5	Predetermined number of cycles

Table A.2 – continued from previous page

Board SN	Revision	Test #	Cycle	Reason for Ending Test
002-00004	3	2	6-12	Tests to study old vs new SSP
002-00005	3	1	1-5	Predetermined number of cycles
002-00006	3	1	1	Installed new set of boards
002-00006	3	2	2-8	Tests to study old vs new SSP
002-00007	3	1	1	Installed new set of boards
002-00007	3	2	2	Test for SiPM cracking
002-00008	3	1	1-7	Predetermined number of cycles
002-00008	3	2	8-29	Tests of board position in little dipper
002-00008	3	3	30	Tests to study old vs new SSP
002-00008	3	4	31	Removed to test hoverboards
002-00009	3	1	1-7	Ended to allow work on little dipper
002-00009	3	2	8-11	Ended to replace boards for new test
002-00009	3	3	12-18	Tests to study old vs new SSP
002-00010	3	1	1-6	Predetermined number of cycles
002-00010	3	2	2-28	Tests of board position in little dipper
002-00010	3	3	29	Removed to test hoverboards
003-00001	3	1	1-6	Predetermined number of cycles
003-00001	3	2	7-10	Installed new set of boards
003-00001	3	3	11	Ended to send board to ANL
003-00003	3	1	1-6	Predetermined number of cycles

Table A.2 – continued from previous page

Board SN	Revision	Test #	Cycle	Reason for Ending Test
003-00003	3	2	7-10	Installed new set of boards
003-00003	3	3	11-17	Ended to allow work on little dipper
003-00003	3	4	18	Single cycle to test for SiPM cracking
003-00003	3	5	19	Removed to test hoverboards
003-00004	3	1	1-6	Predetermined number of cycles
003-00004	3	2	7	Re-test of noisy board
003-00005	3	1	1-5	Predetermined number of cycles
003-00005	3	2	6-9	Installed new set of boards
003-00006	3	1	1-6	Installed new set of boards
003-00006	3	2	7	Re-installed boards in different positions
003-00006	3	3	8	Re-installed boards in different positions
003-00006	3	4	9	Re-installed boards in different positions
003-00006	3	5	10	Re-installed boards in different positions
003-00006	3	6	11	Re-installed boards in different positions
003-00006	3	7	12	Installed new set of boards
003-00006	3	8	13	Test to look for light leak
003-00007	3	1	1-22	Installed new set of boards
003-00007	3	2	23	Re-test of noisy board
003-00007	3	3	24,25	Tests to study old vs new SSP
003-00007	3	4	26, 27	Installed new set of boards

Table A.2 – continued from previous page

Board SN	Revision	Test #	Cycle	Reason for Ending Test
003-00008	3	1	1-22	Installed new set of boards
003-00008	3	2	23	Re-test of noisy board
003-00008	3	3	24,25	Tests to study old vs new SSP
003-00008	3	4	26	Single cycle to test for SiPM cracking
003-00008	3	5	27, 28	Installed new set of boards
003-00009	3	1	1-22	Installed new set of boards
003-00009	3	2	23	Re-test of noisy board
003-00009	3	3	24,25	Tests to study old vs new SSP
003-00009	3	4	26	Single cycle to test for SiPM cracking
003-00009	3	5	27	Removed to test hoverboards
003-00009	3	6	28, 29	Installed new set of boards
003-00010	3	1	1,2	Removed to test hoverboards
004-00001	3	1	1	Removed because SiPMs cracked
004-00002	3	1	1	Removed because SiPMs cracked
004-00003	3	1	1	Removed because SiPMs cracked
004-00004	3	1	1	Removed because SiPMs cracked
004-00006	3	1	1,2	Installed new set of boards
004-00007	3	1	1,2	Installed new set of boards
004-00008	3	1	1,2	Installed new set of boards

TABLE A.2. Testing log for cycle boards.

Board SN	Revision	Test #	Cycle	Reason for Ending Test
002-0018	2	1	1	Ended to send board to ANL
003-0011	2	1	1-20	Predetermined number of cycles
003-0011	2	2	21-32	Installed new set of boards
003-0012	2	1	1	Single cycle to test for SiPM cracking
003-0042	2	1	1-20	Predetermined number of cycles
003-0042	2	2	21-32	Installed new set of boards
004-0003	2	1	1	Ended to send board to ANL
004-0018	2	1	1	Single cycle to test for SiPM cracking
001-0006	3	1	1	Predetermined number of cycles
001-0008	3	1	1	Removed to photograph
001-0008	3	2	2	Removed to photograph
001-0008	3	3	3	Removed to photograph
001-0008	3	4	4	Removed to photograph
001-0008	3	5	5	Removed to photograph
001-0010	3	1	1	Removed to photograph
001-0010	3	2	2	Removed to photograph
001-0010	3	3	3	Removed to photograph
001-0010	3	4	4	Removed to photograph
001-0010	3	5	5	Removed to photograph
002-0004	3	1	1	Predetermined number of cycles

Table A.3 – continued from previous page

Board SN	Revision	Test #	Cycle	Reason for Ending Test
002-0010	3	1	1	Removed to photograph
002-0010	3	2	2	Removed to photograph
002-0010	3	3	3	Removed to photograph
002-0010	3	4	4	Removed to photograph
002-0010	3	5	5	Removed to photograph
002-0016	3	1	1	Removed to photograph
002-0016	3	2	2	Removed to photograph
002-0016	3	3	3	Removed to photograph
002-0016	3	4	4	Removed to photograph
002-0016	3	5	5	Removed to photograph
003-0017	3	1	1	Removed to photograph
003-0017	3	2	2	Removed to photograph
003-0017	3	3	3	Removed to photograph
003-0017	3	4	4	Removed to photograph
003-0017	3	5	5	Removed to photograph
003-0017	3	6	6-21	Installed new set of boards
003-0020	3	1	1	Predetermined number of cycles
003-0032	3	1	1	Removed to photograph
003-0032	3	2	2	Removed to photograph
003-0032	3	3	3	Removed to photograph

Table A.3 – continued from previous page

Board SN	Revision	Test #	Cycle	Reason for Ending Test
003-0032	3	4	4	Removed to photograph
003-0032	3	5	5	Removed to photograph
003-0032	3	6	6-21	Installed new set of boards
003-0042	3	1	1	Removed to photograph
003-0042	3	2	2	Removed to photograph
003-0042	3	3	3	Removed to photograph
003-0042	3	4	4	Removed to photograph
003-0042	3	5	5	Removed to photograph
003-0042	3	6	6-21	Installed new set of boards
003-0046	3	1	1	Removed to photograph
003-0046	3	2	2	Removed to photograph
003-0046	3	3	3	Removed to photograph
003-0046	3	4	4	Removed to photograph
003-0046	3	5	5	Removed to photograph
003-0064	3	1	1	Predetermined number of cycles

TABLE A.3. Testing log for hoverboards.

APPENDIX B

EXCLUDED DATA

Table B.1 contains the list of channels, and corresponding cycles not used in the analysis.

The ranges of channels and cycles are given along with the reason for omission.

Board SN	Channels	Cycles	Reason
00200002	0	8-9	Too few events (dark rate ~ 0)
00200002	0	11-20	Noisy (low gain values)
00200003	10-11	14	Noisy (dark rate >200)
00200004	0-11	9	Noisy (drop in gain and x-talk)
00200004	1	2	Large dark rate (55 Hz) - Analysis 0
00200005	9	1	Noisy (drop in gain and x-talk)
00200006	1-12	all	Noisy
00200007	1-12	all	Noisy
00200005	9	1	Noisy (drop in gain and x-talk)
00200006	all	all	Connectors loose (3rd connector fell off)
00200007	all	all	Only 2 cycles taken (very noisy)
00200008	11	18,21,25	Noisy (gain $\sim 7E5$, dark rate >200)
00200009	all	6-18	Board damaged (lost connector) after cycle 5
00200010	all	1-6	Loose connectors for cycles 1-5 (re-soldered)
00200010	9	all	Noisy
00200010	10	23	Very noisy
00200010	1	28	Noisy

Table B.1 – continued from previous page

Board SN	Channels	Cycles	Reason
00300001	all	1-2	Very noisy
00300003	1	6	Noisy
00300003	1-10	2	Noisy
00300003	6	3	Noisy
00300003	9	7	Noisy
00300003	4	11-18	Noisy
00300003	1	11-19	Noisy
00300003	3-4	19	Noisy

TABLE B.1. Excluded channels (cycle boards) not used in analysis along with rationale for exclusion.

APPENDIX C

PLOTS OF RESULTS FROM THERMAL CYCLING

These plots show the completed testing results from our thermal cycle testing. Each tested board is given a separate plot, and each board contains 12 SiPMs. Each SiPM is listed as a separate channel in the data, labeled 0 through 11. The gain, dark rate, and crosstalk are plotted against cycle number. The results show consistent SiPM characteristics over many thermal cycles, and there are no obvious signs of thermal damage.

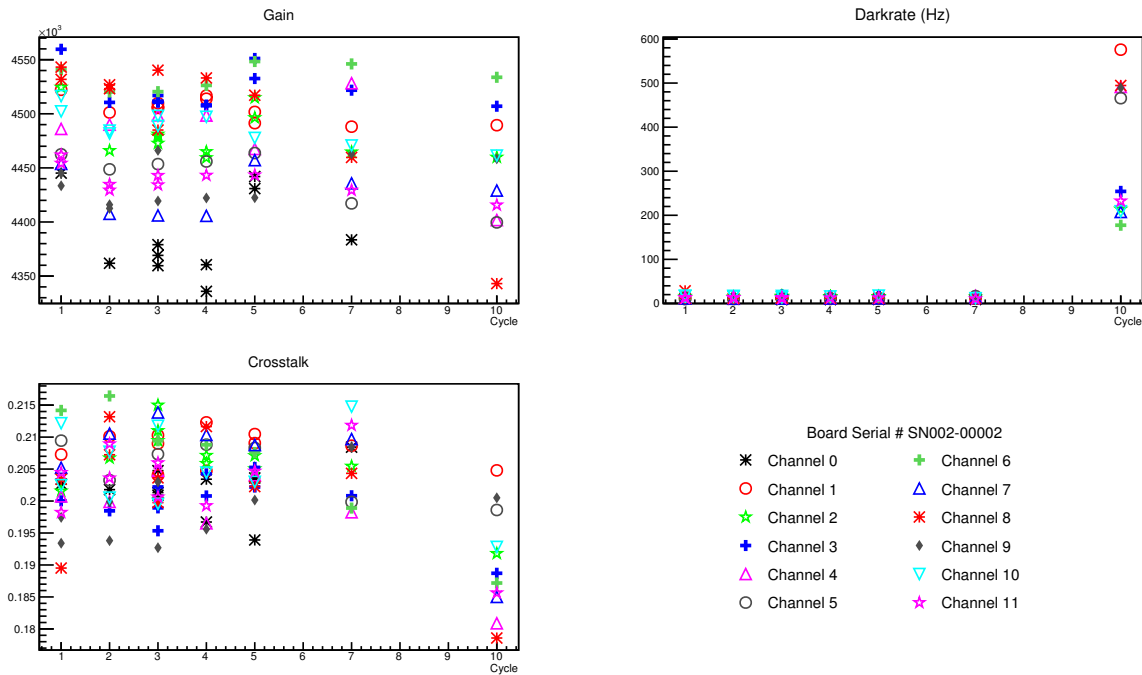


FIGURE C.1. 03-600365C-SN00200002

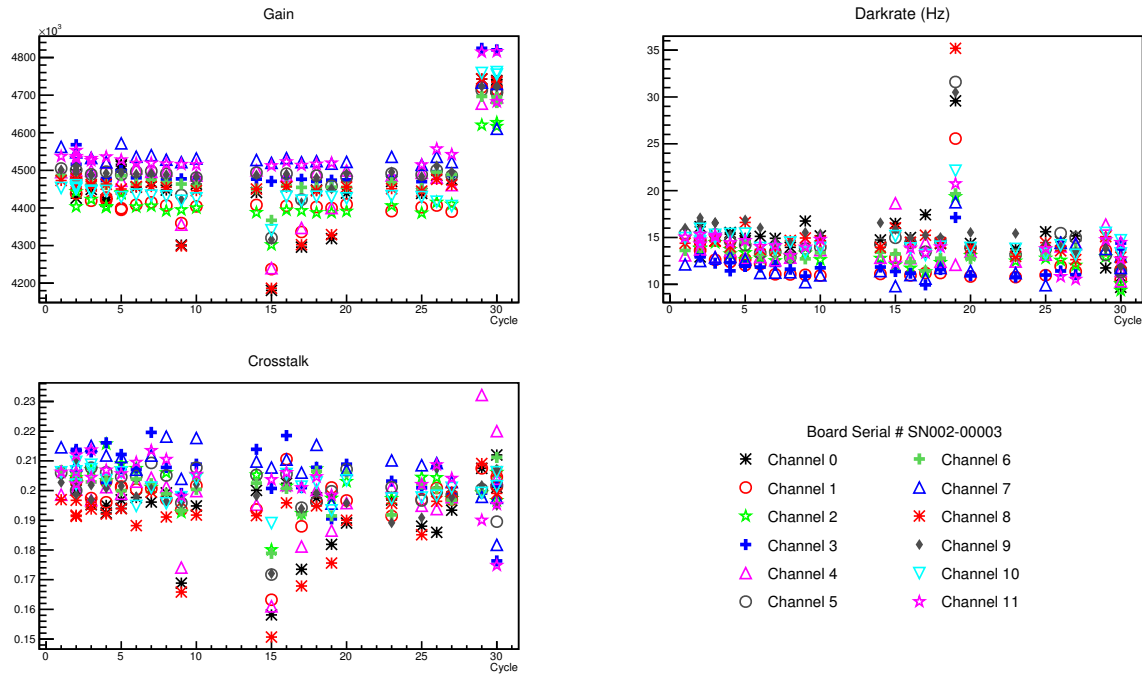


FIGURE C.2. 03-600365C-SN00200003

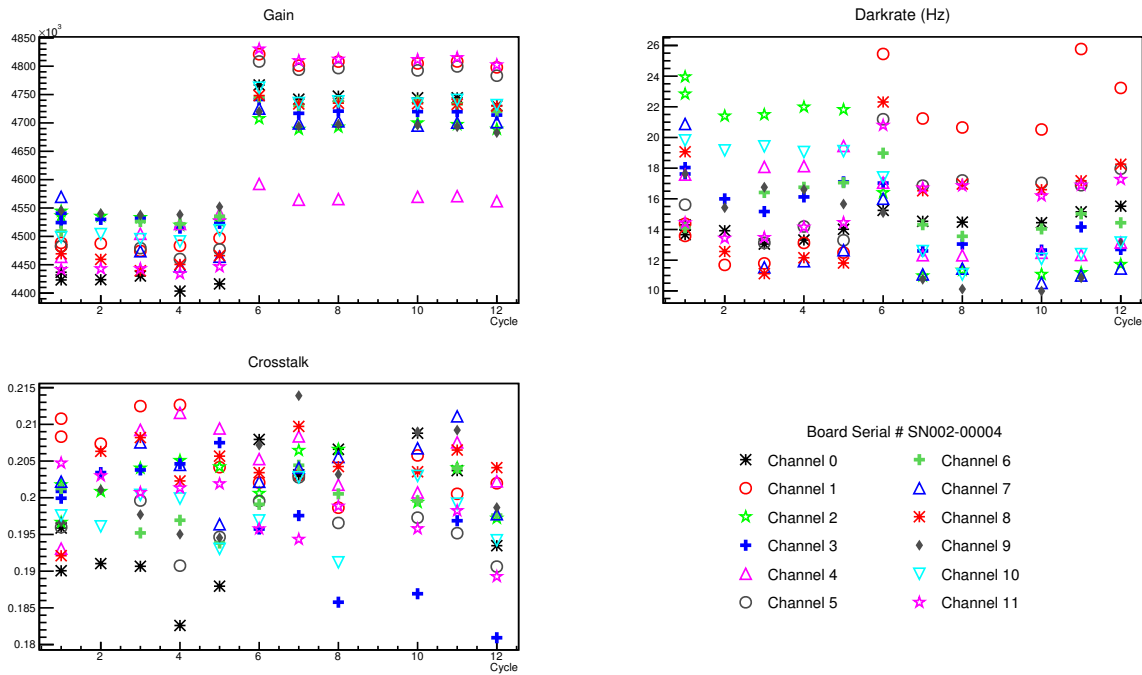


FIGURE C.3. 03-600365C-SN00200004

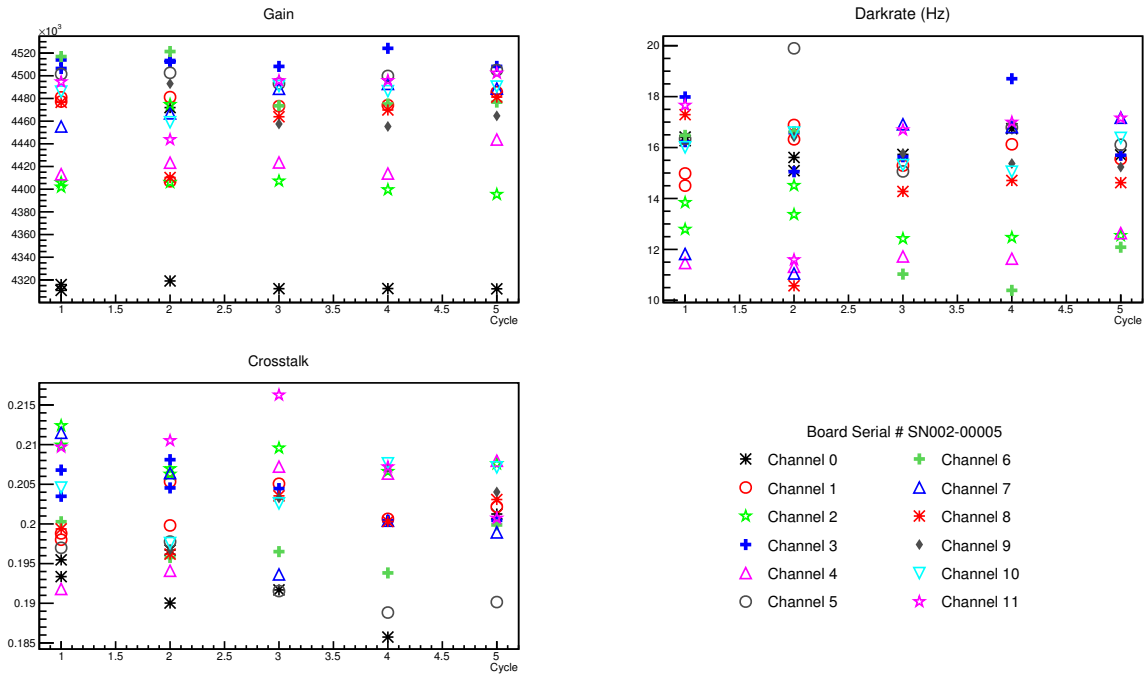


FIGURE C.4. 03-600365C-SN00200005

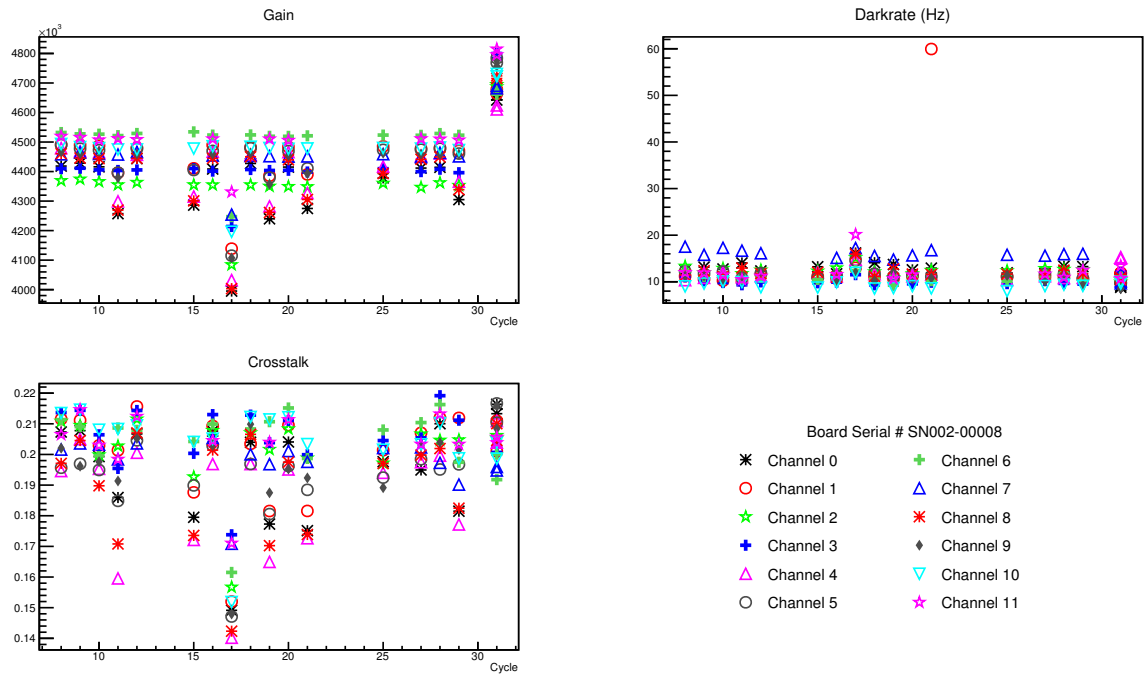


FIGURE C.5. 03-600365C-SN00200008

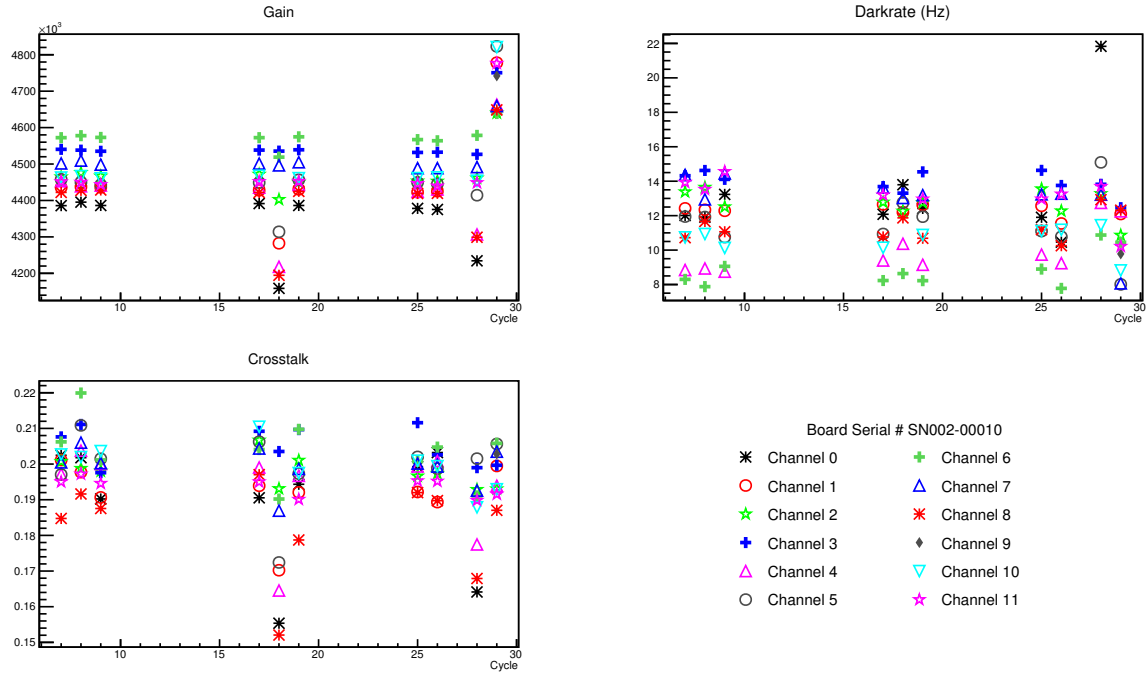


FIGURE C.6. 03-600365C-SN00200010

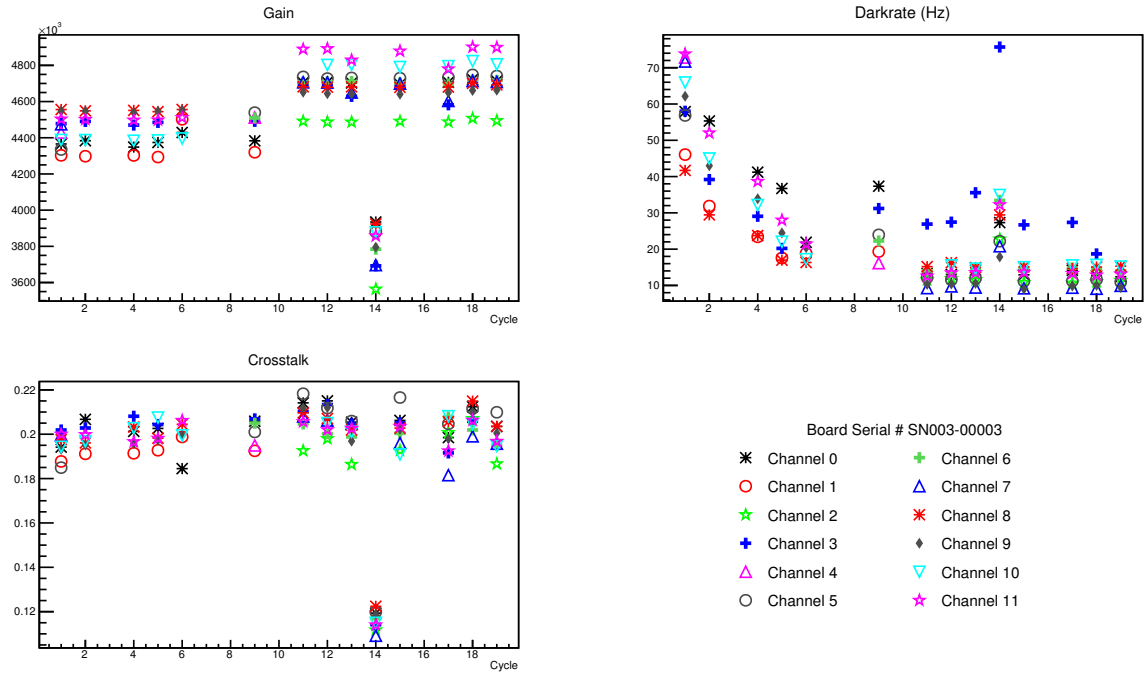


FIGURE C.7. 03-600365C-SN00300003

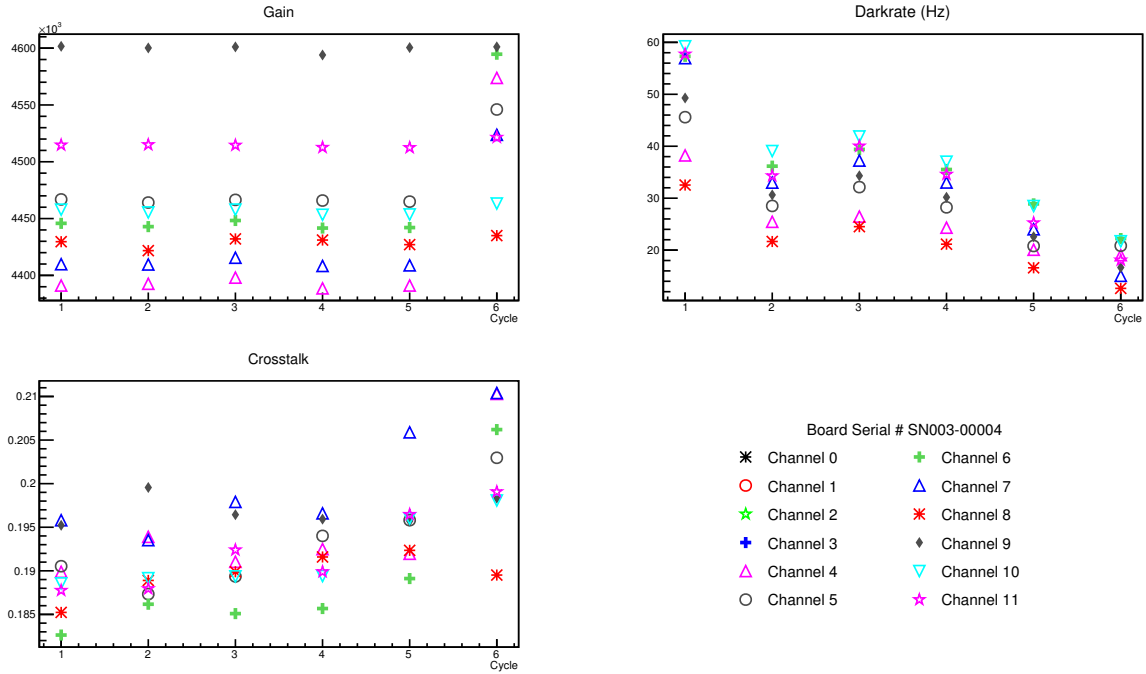


FIGURE C.8. 03-600365C-SN00300004

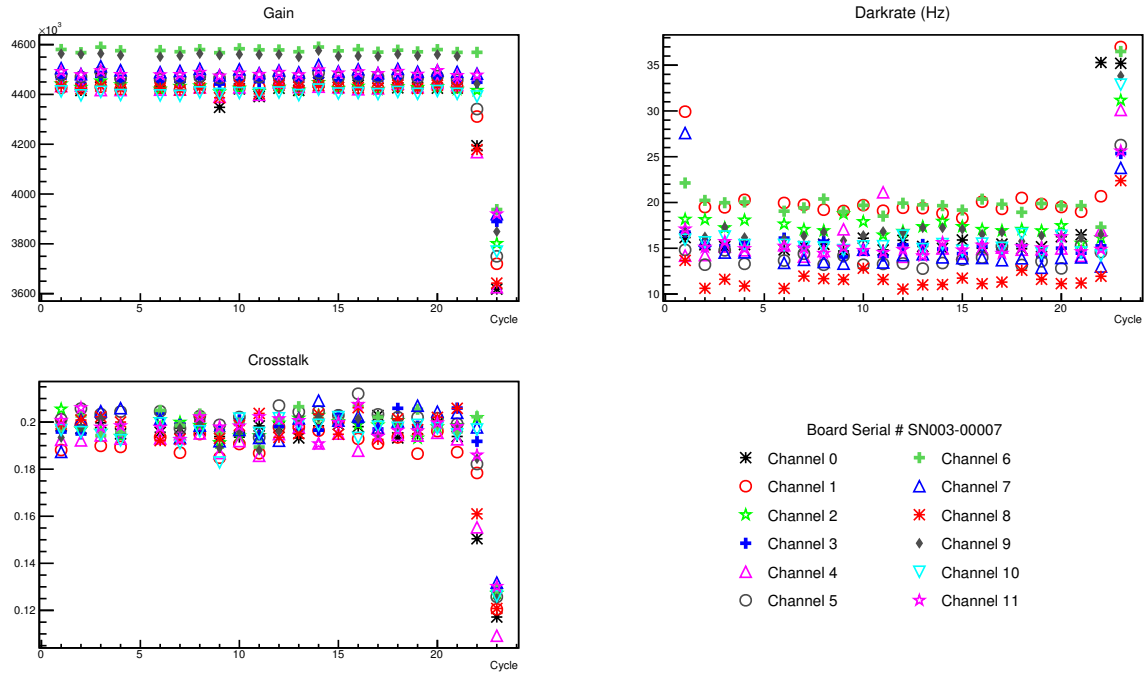


FIGURE C.9. 03-600365C-SN00300007

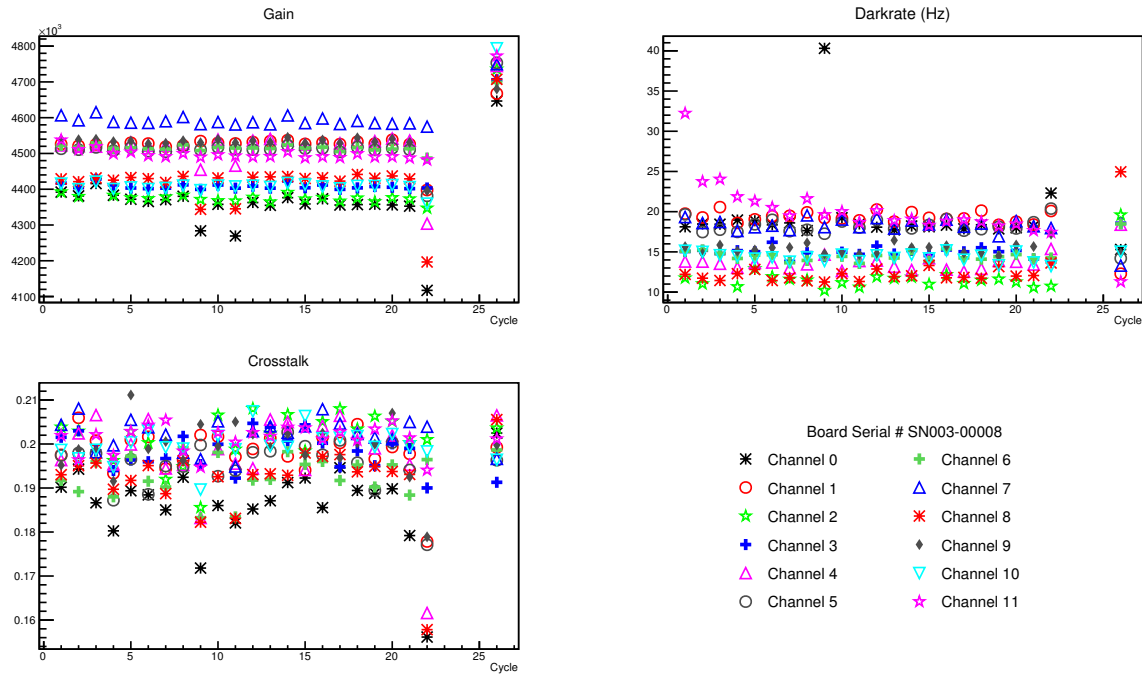


FIGURE C.10. 03-600365C-SN00300008

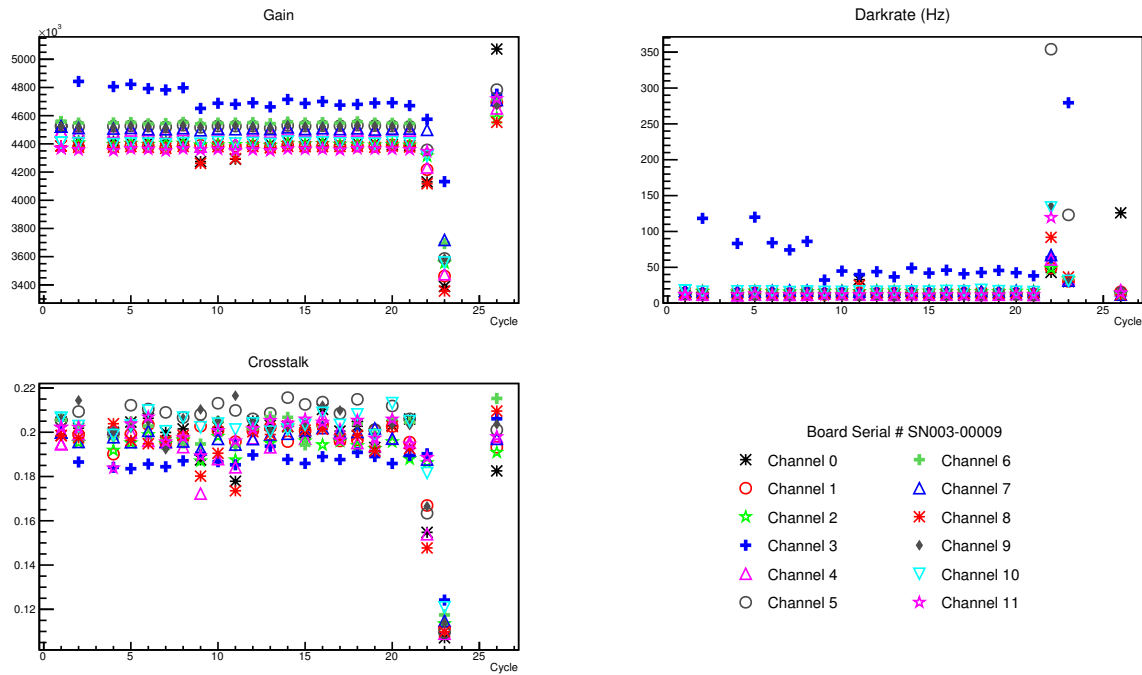


FIGURE C.11. 03-600365C-SN00300009

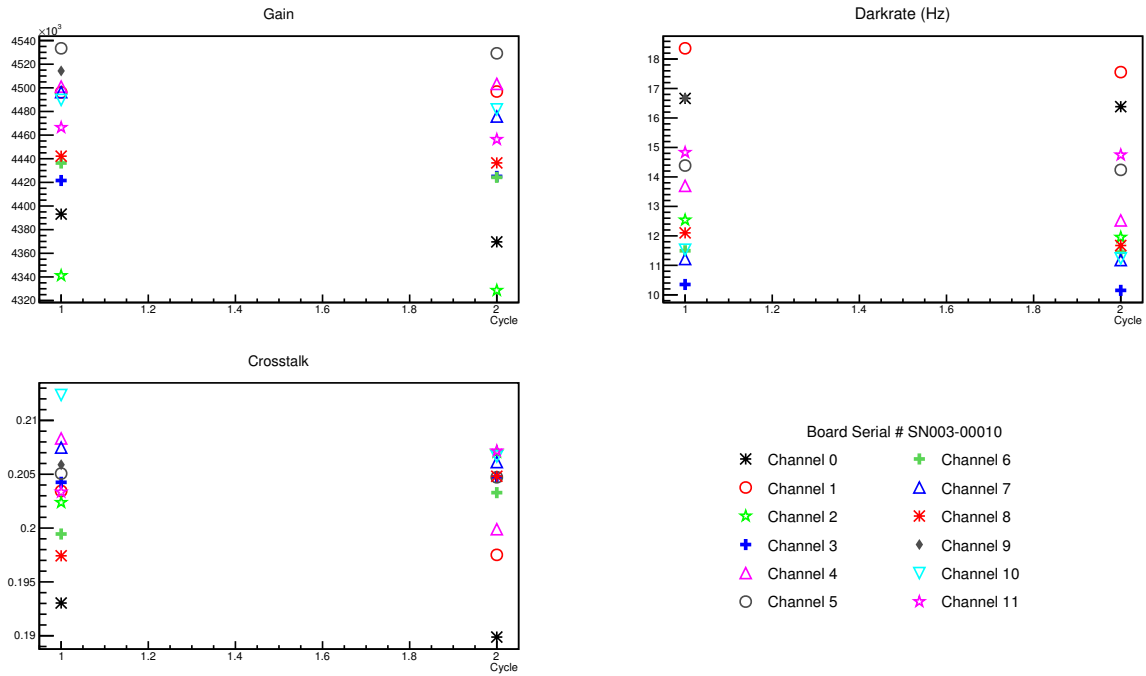


FIGURE C.12. 03-600365C-SN00300010